

INFORMATION TO USERS

This manuscript has been reproduced from the microfilm master. UMI films the text directly from the original or copy submitted. Thus, some thesis and dissertation copies are in typewriter face, while others may be from any type of computer printer.

The quality of this reproduction is dependent upon the quality of the copy submitted. Broken or indistinct print, colored or poor quality illustrations and photographs, print bleedthrough, substandard margins, and improper alignment can adversely affect reproduction.

In the unlikely event that the author did not send UMI a complete manuscript and there are missing pages, these will be noted. Also, if unauthorized copyright material had to be removed, a note will indicate the deletion.

Oversize materials (e.g., maps, drawings, charts) are reproduced by sectioning the original, beginning at the upper left-hand corner and continuing from left to right in equal sections with small overlaps.

Photographs included in the original manuscript have been reproduced xerographically in this copy. Higher quality 6" x 9" black and white photographic prints are available for any photographs or illustrations appearing in this copy for an additional charge. Contact UMI directly to order.

Bell & Howell Information and Learning
300 North Zeeb Road, Ann Arbor, MI 48106-1346 USA

UMI[®]
800-521-0600

**TOWARD CFD-BASED CORRELATIONS FOR
A SINGLE-STAGE HIGH-PRESSURE
TRANSONIC TURBINE**

IYAD AKEL

A Thesis
in
The Department
of
Mechanical Engineering

Presented in Partial Fulfillment of the Requirements
for the Degree of Master of Applied Science at
Concordia University
Montréal, Québec, Canada

April 1999

© Iyad Akel, 1999



National Library
of Canada

Acquisitions and
Bibliographic Services

395 Wellington Street
Ottawa ON K1A 0N4
Canada

Bibliothèque nationale
du Canada

Acquisitions et
services bibliographiques

395, rue Wellington
Ottawa ON K1A 0N4
Canada

Your file Votre référence

Our file Notre référence

The author has granted a non-exclusive licence allowing the National Library of Canada to reproduce, loan, distribute or sell copies of this thesis in microform, paper or electronic formats.

The author retains ownership of the copyright in this thesis. Neither the thesis nor substantial extracts from it may be printed or otherwise reproduced without the author's permission.

L'auteur a accordé une licence non exclusive permettant à la Bibliothèque nationale du Canada de reproduire, prêter, distribuer ou vendre des copies de cette thèse sous la forme de microfiche/film, de reproduction sur papier ou sur format électronique.

L'auteur conserve la propriété du droit d'auteur qui protège cette thèse. Ni la thèse ni des extraits substantiels de celle-ci ne doivent être imprimés ou autrement reproduits sans son autorisation.

0-612-43550-4

ABSTRACT

TOWARD CFD-BASED CORRELATIONS FOR A SINGLE-STAGE HIGH-PRESSURE TRANSONIC TURBINE

Iyad Akel

Correlations are of great importance in the preliminary design of a gas turbine engine. They are useful to determine the efficiency and thus the Specific Fuel Consumption (SFC) of the engine, before even having blade geometries. Also, correlations play a very important role in the understanding of the behavior (performance) of the engine, under different operating conditions.

Since most correlations are obtained from expensive rig tests and cascades, and since cascades do not represent all the flow phenomena in actual engines, the necessity of finding less expensive and more realistic representations of the actual flow phenomena is becoming more and more important.

With the great advances in Computational Fluid Dynamics (CFD), CFD is becoming the tool of choice in the analysis of complex flow phenomena, such as that in gas turbine engines.

In a novel cost-effective approach, it is proposed to use CFD as the experimental test-cell to generate these correlations and to extend their regime of applicability.

Using a 3-D finite element viscous, compressible, turbulent code, developed jointly by Concordia University CFD laboratory and Pratt & Whitney Canada, CFD-based correlations for a high-pressure transonic turbine will be created and validated against Cold Flow Turbine Rig test data. This will be done by studying the effect of variation of four design and off-design parameters, on the performance characteristics of the turbine stage.

Acknowledgments

I would like to thank my advisor Dr. Wagdi Habashi for his guidance and support during the project, and for his very constructive remarks on the writing of this thesis. Also, my special thanks go to my co-supervisor Dr. Hany Moustapha for his technical support about the project and the writing of the thesis, and for permitting to me the use of Pratt & Whitney Canada (P&WC) facilities and super-computers. I feel privileged to have had such great advisors with a world wide reputation.

Since the entire work of this thesis has been carried out at P&WC, I would like to thank all the members of P&WC's CFD group and their leader Dr. Michel Robichaud, and particularly Mr. (to be Dr.) Mohamad Sleiman for his helpful technical expertise. Also, I would like to express my gratitude to P&WC's turbine group, and especially Dr. Jean-Paul Lavoie for his technical expertise and very helpful suggestions, and for his particular sense of humor. My thanks go also to Dr. Michael W. Krieger, for his very useful comments and remarks on the thesis.

Also, I would like to extend my thanks to all the members of Concordia CFD Lab members for the nice and friendly environment that has spawned great work,

with camaraderie.

Last but not least, I would like to express my extreme and deepest thanks to my parents, Ghassan & Yvonne, and to my brothers Riad & Nehad (we are **THE THREE MOUSQUATEERS**), for their continuous encouragement and support throughout all of my studies.

Thus, I would like to dedicate this modest work to my great and unique family, since they have taught me what none neither nothing else could teach me

Also, I would like to dedicate this very modest work, to my country **SYRIA**, **MOTHERLAND OF CIVILIZATIONS** and **FIRST ALPHABET IN THE HISTORY OF HUMANITY**, and to my hometown **DAMASCUS**, **THE OLDEST ALWAYS INHABITANT CITY IN THE WORLD**.

“Every cultured man has two homelands: The first is his country of birth; the second is SYRIA.”

said by a great historian.

Table of Contents

List of Figures	ix
List of Tables	xii
Nomenclature	xiii
1. Introduction	1
1.1. Literature review	5
1.2. Purpose of the present work	8
1.3. Overview of the thesis	9
2. The test cases	16
2.1. Outline of test cases	16
2.2. Description of boundary conditions	18
2.3. CFD set-up and overview of the code	22
3. Parameters studied	31
3.1. Effect of Tip Clearance (clearance/span) on performance characteristic of high-pressure turbine stage	31
3.1.1. Tip leakage vortex	41
3.2. Effect of Blade Speed (RPM) on performance characteristics of high- pressure turbine stage	50
3.3. Effect of Pressure Ratio (PR) on performance characteristics of high- pressure turbine stage	58
3.4. Effect of Vane Stagger Angle on performance characteristics of high- pressure turbine stage	66
4. Discussions	72
4.1. Accomplishments and Conclusion	72
4.2. Future work and suggestions	75

References	77
Appendices	87
Appendix A: Turbine & gas path detailed geometry	88
Appendix B: Sample (the design case) thermodynamic variables variation through out each of the vane and the blade passage	90

List of Figures

Figure 1-1. Gas turbine design steps	11
Figure 1-2. Simple gas turbine system	12
Figure 1-3 Turboprop & turbofan engines: (a) cross section of a P&WC turboprop engine, (b) artistic representation of a turbofan engine	12
Figure 1-4 Large and mid size turbofan engines	13
Figure 1-5 Axial turbine blade nomenclature and velocity triangle	14
Figure 1-6 Aerodynamic design procedure for a gas turbine	15
Figure 2.2-1 Turbine stage actual geometry	26
Figure 2.2-2 Vane and Blade geometry	26
Figure 2.2-3 Location of analysis stations	27
Figure 2.3-1 Vane computational mesh	28
Figure 2.3-2 Blade computational mesh	29
Figure 2.3-3 Regions descriptions	29
Figure 2.3-4 CFD analysis procedures	30
Figure 3.1-1 NS3D predictions for the variation of stage efficiency vs. Blade tip clearance	34
Figure 3.1-2 NS3D predictions for vane mid-span Mach number distribution, for all the tip clearances	35
Figure 3.1-3 NS3D predictions for vane Mach number distribution at 99% span, for all the tip clearances	35
Figure 3.1-4 NS3D predictions for blade Mach number distribution at different span locations, for all the tip clearances	36
Figure 3.1-5 Views of the tip leakage vortex for the three blade tip clearances as predicted by NS3D	39

Figure 3.1-6 NS3D predictions for averaged stage reaction, for all the tip clearances	39
Figure 3.1.1-1 NS3D predictions for the 2.5% tip clearance/span blade Mach number distribution at different span locations	44
Figure 3.1.1-2 Static pressure contour lines: (a) at plane A (45.55% chord), (b) at plane B (50.70% chord), (c) at plane C (99.50% chord)	44
Figure 3.1.1-3 Velocity vectors: (a) at plane A, (b) at plane B, (c) at plane C .	45
Figure 3.1.1-4 Mach number contour lines: (a) at plane A, (b) at plane B, (c) at plane C	46
Figure 3.1.1-5 Entropy contour lines: (a) at plane A, (b) at plane B, (c) at plane C	46
Figure 3.1.1-6 Vortices merge: Entropy distribution & contour lines: (a) two vortices at plane D (TE + 0.16 chord), (b) one vortex (merged vortices) at plane E (TE + 0.41 chord)	47
Figure 3.1.1-7 Evolution of the vortex: Entropy distribution at different planes F(TE), G(TE + 1 chord), H(TE + 2 chords), I(TE + 3 chords) and J(TE + 3.47 chords)	48
Figure 3.1.1-8 Entropy distribution and contour lines: (a) at plane F, (b) at plane G, (c) at plane H, (d) at plane I, (e) at plane J	49
Figure 3.2-1 Effect of varying blade speed on the velocity triangle	54
Figure 3.2-2 NS3D predictions for the variation of stage efficiency vs. Blade speed	54
Figure 3.2-3 NS3D predictions for vane mid-span Mach number distribution, for all blade speeds	55
Figure 3.2-4 NS3D predictions for blade mid-span Mach number distribution, for all blade speeds	55
Figure 3.2-5 NS3D predictions for averaged stage reaction, for all blade speeds	56
Figure 3.3-1 Effect of varying pressure ratio on the velocity triangle	62

Figure 3.3-2 NS3D predictions for the variation of stage efficiency vs. Stage pressure ratio	62
Figure 3.3-3 NS3D predictions for vane mid-span Mach number distribution, for the six PR's studied	63
Figure 3.3-4 NS3D predictions for blade mid-span Mach number distribution, for the six PR's studied	63
Figure 3.3-5 NS3D predictions for blade in and out relative swirl, for the range of stage pressure ratios studied	64
Figure 3.3-6 NS3D predictions for average stage reaction, for the range of stage pressure ratios studied	64
Figure 3.4-1 NS3D predictions of stage efficiency for the effect of closing vane stagger angle by 0.8°	69
Figure 3.4-2 NS3D predictions for vane mid-span Mach number distribution, for the two speeds and vane stagger angles	69
Figure 3.4-3 NS3D predictions for blade mid-span Mach number distribution, for the two speeds and vane stagger angles	70
Figure 3.4-4 NS3D predictions for averaged stage reaction, for the two speeds and vane stagger angles	70

List of Tables

Table 2.2-1	Turbine stage characteristics and boundary conditions	25
Table 2.3-1	Mesh details	25
Table 3.1-1	Stage efficiency of the four blade tip clearances	40
Table 3.1-2	Stage detailed analysis for all the tip clearances studied	40
Table 3.1-3	Influence of blade tip clearance on the stage reaction	40
Table 3.2-1	Stage efficiency of the six blade speeds	57
Table 3.2-2	Stage detailed analysis for all the blade speeds studied	57
Table 3.2-3	Influence of blade speed on stage reaction	57
Table 3.3-1	Stage efficiency for the six stage pressure ratios	65
Table 3.3-2	Stage detailed analysis for the range of pressure ratios studied ..	65
Table 3.3-3	Influence of stage pressure ratio on turbine stage reaction	65
Table 3.4-1	Stage efficiency and comparison for the closed and unclosed vane, at the two speeds	71
Table 3.4-2	Stage detailed analysis and comparison for the closed and unclosed vane, at the two speeds	71
Table 3.4-3	Influence of vane stagger angle and blade speed on stage reaction	71

Nomenclature


<i>Blade</i>	rotor (but could also be stator)
<i>CFTR</i>	cold flow turbine rig
<i>C</i>	absolute velocity
<i>Cr</i>	radial velocity
<i>Cx</i>	axial velocity
<i>DELP/P</i>	delta P_t/P_t (loss, see equation 2.2-3)
<i>HPT</i>	high-pressure turbine
<i>ITD</i>	inter turbine duct
<i>LE</i>	leading edge
<i>M</i>	Mach number
$m\sqrt{T_t/P_t}$	flow capacity
<i>N</i>	rotor rotational speed (rpm)
N/\sqrt{T}	normalized speed (rpm/ $\sqrt{^\circ\text{R}}$)
<i>Nozzle</i>	stator (see vane also)
<i>NS3D</i>	the 3-D viscous flow solver used
<i>p</i>	static pressure (psi)
<i>PR</i>	pressure ratio
<i>P_t</i>	total pressure (psi)
<i>R</i>	degree of reaction
$^\circ\text{R}$	degrees Rankin (temperature)
<i>SFC</i>	specific fuel consumption
<i>T</i>	static temperature ($^\circ\text{R}$)
<i>TE</i>	trailing edge
<i>tpclr</i>	tip clearance

T_t	total temperature ($^{\circ}\text{R}$)
U	rotor rotational speed
V	relative velocity
<i>Vane</i>	stator (see nozzle also)

Greek symbols

α	absolute gas angle
β	relative gas angle
γ	ratio of specific heats
η	isentropic efficiency
Δ	change in a variable
ϕ	flow cone angle (C_r/C_x)

Subscripts

1		Station number (see figure 2.2-3)
1a		
2		
2a		
3		
4		
4a		

<i>abs</i>	absolute value
<i>des</i>	design
<i>r</i>	radial
<i>rel</i>	relative value

<i>s</i>	static
<i>t</i>	total (see tot also)
<i>tot</i>	total (see t also)
<i>x</i>	axial

Superscripts

°	degrees
---	---------

1. Introduction

The design of a gas turbine engine is a fairly lengthy and complex process, and thus, it requires several months (or in certain cases years) of detailed analysis and testing. A simplified schematic of a gas turbine design is presented in figure 1-1.

Due to the ferocious competition in the gas turbine industry, and to the continuous advances in design techniques, nowadays, a minor difference in engine total efficiency can make or break engine manufacturers. Because of that, each component of the gas turbine engine undergoes extensive detailed analysis and experiments to yield the maximum efficiency possible.

A good example of a leading gas turbine manufacturer is Pratt & Whitney Canada (P&WC), a world leader in small gas turbines. Due to the distinct collaborations between Concordia's CFD laboratory and P&WC, I had the privilege to carry out the entire work of the present thesis in this very advanced company.

A gas turbine system is composed of three major components: compressor, combustion chamber and a turbine that drives the compressor, as shown in

figure 1-2. The working fluid is compressed in the compressor, heated in the combustion chamber and then expanded in the turbine, thus producing power.

In practice, losses occur in the components causing the net power to drop and the efficiency of the system to decrease. To account for the decrease in power, more fuel is needed to be burned, causing the specific fuel consumption (SFC) of the plant to increase. To improve engine efficiency, each component is designed to work at its highest possible efficiency for the required operating conditions of the engine (the design condition).

For the case of gas turbine engines used for aircraft propulsion (see figure 1-3 & 1-4), the working envelope of the engine is very large, and the operating conditions will vary from take-off, climb, cruise, descent and landing. Thus, considerations will be made during design, to account for the penalties of off-design operating conditions, and to keep the efficiency of each component (and thus, the engine) reasonably high.

The work presented in this thesis focuses on multistage axial turbines. A turbine stage is composed of a row of stators ("vanes" and "nozzles"), followed by a row of rotors (also known as "blades", in this thesis, this term is very often used). The number of stages depends on many factors dictated by the application and design requirements of the engine. A representation of a typical turbine stage

and velocity triangle (representation of velocity vectors on the stage that is used in the analysis of turbomachines) is shown in figure 1-5.

The aerodynamic design of a turbine stage is an elaborate process as seen in the schematic of figure 1-6. In order to design an efficient turbine, a very good knowledge of its change in performance at different operating conditions is extremely important. This kind of information can be obtained from correlated experimental results of many test cases run on turbines. As it can be seen from figure 1-6, the first step in the design (preliminary design) is based on correlations (mean line design). Correlations are used to predict the efficiency of the turbine (and thus, the SFC of the engine). They are also useful in evaluating the behaviour of a gas turbine engine under varying conditions. They assist in predicting aerodynamic losses and in understanding the effect of design changes and off-design conditions on the efficiency of a power plant. Such correlations are needed at all stages of the design of turbomachines. While Computational Fluid Dynamics (CFD) is supplanting such methods in the 3-D aerodynamic design of components, the fact is that correlations will still be needed for a long time to come for the 1-D (mean-line) and 2-D (Through-Flow) preliminary analysis of turbomachines. Such 1-D and 2-D design steps are an essential feature of the overall design process of a turbomachine.

These correlations require extensive and costly experiments. If carried on actual engines, this would be a prohibitively expensive operation. Thus, most test data used for the creation of the correlations are obtained from Cascade or Cold Flow Turbine Rigs (CFTR). Unfortunately, cascades predictions are not free from experimental errors, and they apply to cascades rather than to the actual turbines, since the flow in a turbine is much more complex than in a cascade. The real situation is one of three-dimensional flow, high radial pressure gradients, centrifugal and Coriolis forces, and unsteadiness and high turbulence levels [20].

Thus, the necessity of using less expensive and more complete tools to get good correlations is very important. That powerful tool that could replace experiments at much lower cost is Computational Fluid Dynamics (CFD). This fact is becoming more true with time due to the significant progress and affordability of computational tools. But also, CFD has its own source of error that should not be ignored, and its accuracy is dependent on the equations and the way the boundary conditions are applied in the modelling.

In a novel approach to generating correlations, it is proposed to use CFD. At Pratt & Whitney Canada (P&WC), with the co-operation of Concordia's CFD laboratory, 3-D unsteady viscous analysis codes for multistage turbomachines are a reality. It is proposed that:

- a) These codes be used to confirm and verify existing correlations used in the gas turbine industry,
- b) Once a degree of confidence is achieved, it is suggested to use these sophisticated codes to build correlations outside the envelope of the existing experimental set-ups, thus edging towards a real-time numerical test cell.

1.1. Literature review

A wealth of experimental data on turbines has been generated in the literature to improve the physical understanding of loss mechanisms, update design and loss correlations used in the preliminary design phase, explore new design concepts and generate test cases for CFD validation. Comparison between such tests and analysis has been traditionally based on 3-D inviscid codes, with no serious attempt to use 3-D viscous analysis for predicting turbine aerodynamic losses and efficiency or for developing new design concepts.

In the last 50 years, many turbine correlations, obtained from cascades or rig tests, have been developed: Soderberg (1949), Stewart (1960) [52], Traupel (1966, revised in 1977), Balijé and Binsley (1968) [6], Muktarov and Krichiakiene (1969), Craig and Cox (1971) [15], Denton (1973) [20], Hultsch and Sauer (1978), and many others. Most of these methods focused mostly on design point conditions.

Probably the most complete and comprehensive method of predicting the design and off-design performance of axial turbines is that due to Ainley and Mathieson (1952) [2]. This method was first modified by Dunham and Came (AMDC) (1970) [12], and then, followed by another refinement by Kacker and Okapuu (1981) [41]. The improvements to the Ainley and Mathieson correlations were performed on profile, secondary and tip clearance losses coefficient at design conditions.

Moustapha et al. (1990) [55] then revised the available correlations for profile and secondary losses at off-design conditions. Lately, their correlations have been improved by Moustapha et al. (1995) [5] with respect to the influence of leading-edge geometry on profile losses at off-design incidence.

For single stage high-pressure ratio turbines, most of the analyses carried out in the past, have also been carried out experimentally. Ewen et al. (1973) tested a lightly loaded ($\Delta H/U^2 = 1.2$) turbine, with a PR of 3.4 [23]. Okapuu (1974) studied the performance of a turbine of PR of 3.9 and $\Delta H/U^2 = 1.5$ by studying the effect of reaction, rotor tip clearance and nozzle and rotor aspect ratio [40]. Liu et al. (1979) discussed the analysis of a low aspect ratio turbine with a PR of 3 and a loading of $\Delta H/U^2 = 1.7$ [33]. The collaboration between P&WC and NASA in the Energy Efficient Engine (E³) program has resulted in the testing done by

Crow et al. (1980), on a turbine of PR of 4 ($\Delta H/U^2 = 1.6$), with uncooled and cooled vane and rotor [16]. Bryce et al. (1985) studied the performance of a cooled (stator & rotor cooling), high pressure ratio (PR = 4.5), high stage loading ($\Delta H/U^2 = 2.1$ turbine [10]. Takagi (1986) investigated the performance of a high stage loading ($\Delta H/U^2 = 2.1$) turbine with PR = 4.16 at design and off-design conditions [54]. Moustapha et al. (1987) investigated the effect of vane contouring and rotor loading on the performance of the nozzle, the rotor and the stage of a highly loaded ($\Delta H/U^2 = 2.5$) turbine with a PR of 3.8 [59].

All of the above investigations mainly focused on design point performance (except Takagi, 1986). Of the many papers reporting on single stage transonic turbines, few studied the off-design performance. Recently, some papers investigated the off-design performance characteristic such as Vlasic et al. (1996) [56]. They studied a cooled high-pressure ratio (PR = 5) transonic turbine. Their work focused on the effect of speed and PR on the performance of the turbine. They showed that off-design operation has a significant effect on turbine efficiency.

Perhaps the most recent paper on off-design performance analysis on a single stage transonic turbine is that of Woinowsky-Krieger et al. (1998) [60]. They reported on the stage aerodynamic design and testing at off-design conditions.

They studied the effect of PR, speed (rpm) and Reynolds number over a wide range. Their results reasonably match the results of a 3-D viscous solver.

1.2. Purpose of the present work

Due to the enormous progress in computing technology and progress in techniques for solving large scale problems, CFD has become more and more a powerful and essential tool in the design and analysis of gas turbine engines. CFD's ultimate goal should never be to replace experiments in the design, but to work hand in hand so that each is used in its optimal applicability area.

The purpose of the present thesis is quite different from the traditional applications of CFD. It is an attempt at demonstrating the capacity of a CFD code to supplement and eventually replace experiments in creating simple correlations (that is the capacity of the code to determine the effect of the variations of design parameters on the performance of the turbine), that are of great importance in the preliminary design stage of gas turbine engines. It is also to show the power and usefulness of a CFD code to investigate the potential causes of losses in very complex flows, such as in a very loaded single stage high-pressure transonic turbine.

It is worth mentioning here, that the flow solver used in the present work is under continuing development jointly by Pratt & Whitney Canada and Concordia University (CFD Laboratory). The results obtained in this work are therefore also considered as a code validation exercise, and certainly the first results obtained from this code for turbines. Thus, this work represents the first step development of the CFD methodology that will be used in the future for design of engines, and for the development and numerical testing of new design concepts.

1.3. Overview of the thesis

In the first place, a summary of the test cases (section 2.1) will be given. Then the boundary conditions (section 2.2) will be described. Before starting the analysis, the CFD set-up and a brief description of the code (section 2.3) will be given.

As a first case, tip clearance to span ratio will be analyzed by taking different tip clearance to span ratios and studying their effect on the performance of the turbine. Also, the tip leakage vortex (section 3.1.1) will be studied, and the relation between the tip clearance/span and the number and strength of the tip leakage vortices will be verified and investigated.

Following this, the effect of blade speed (section 3.2) on the performance of the turbine will be studied. Detailed 3-D viscous analyses to predict turbine aerodynamic losses are performed and the results compared to test data and to a turbine correlation model. Furthermore, the effect of turbine pressure ratio (section 3.3) on performance is analysed and compared to experimental values as well as to correlations.

Finally, the effects of vane stagger angle (section 3.4) on turbine aerodynamic losses will be investigated by detailed 3-D viscous analyses. As a conclusion, the results will be discussed (section 4.1) and suggestions (section 4.2) made for future work.

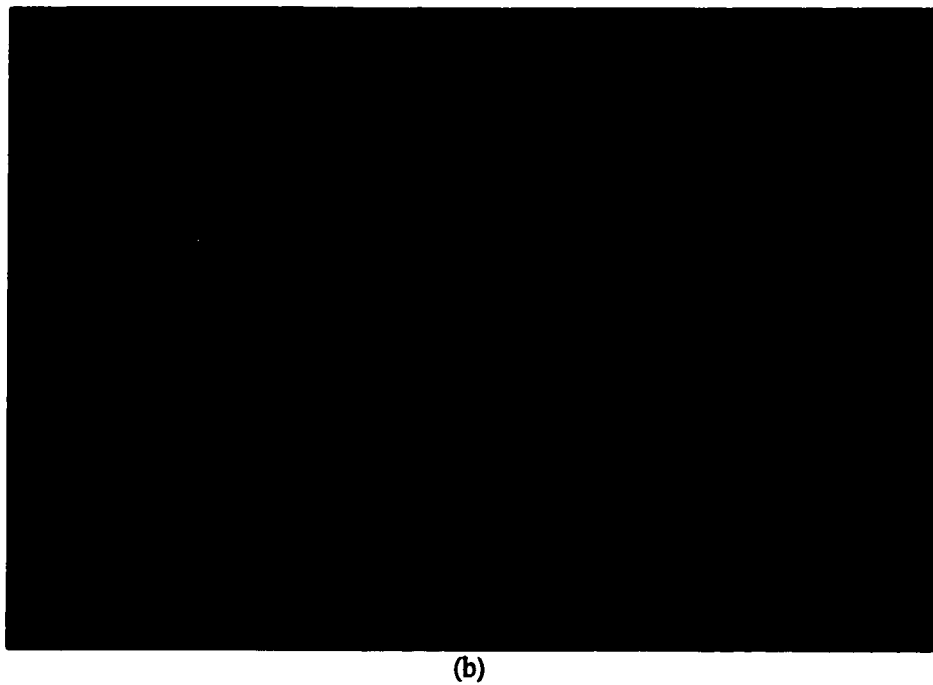
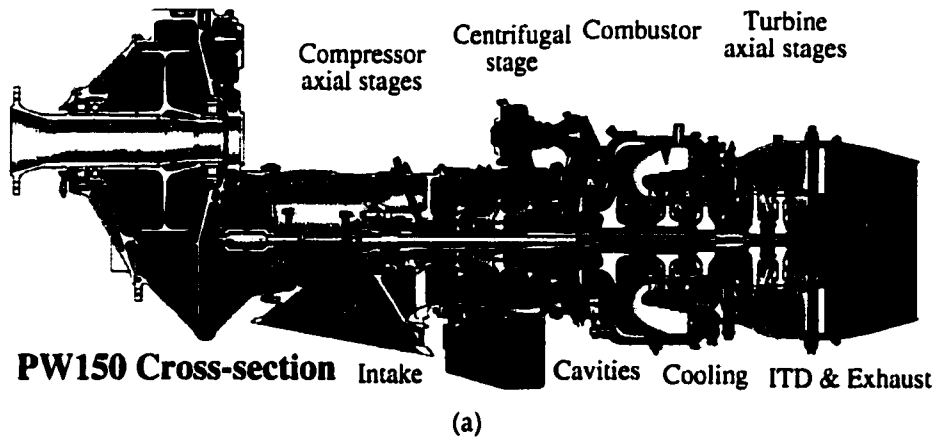
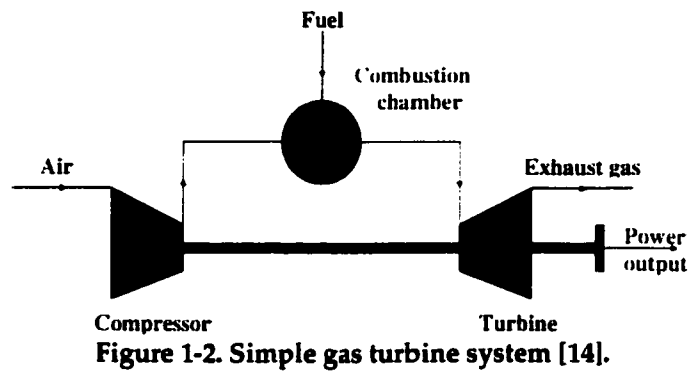


Figure 1-3 Turboprop & turbojet engines: (a) cross section of a P&WC turboprop engine, (b) artistic representation of a turbojet engine.

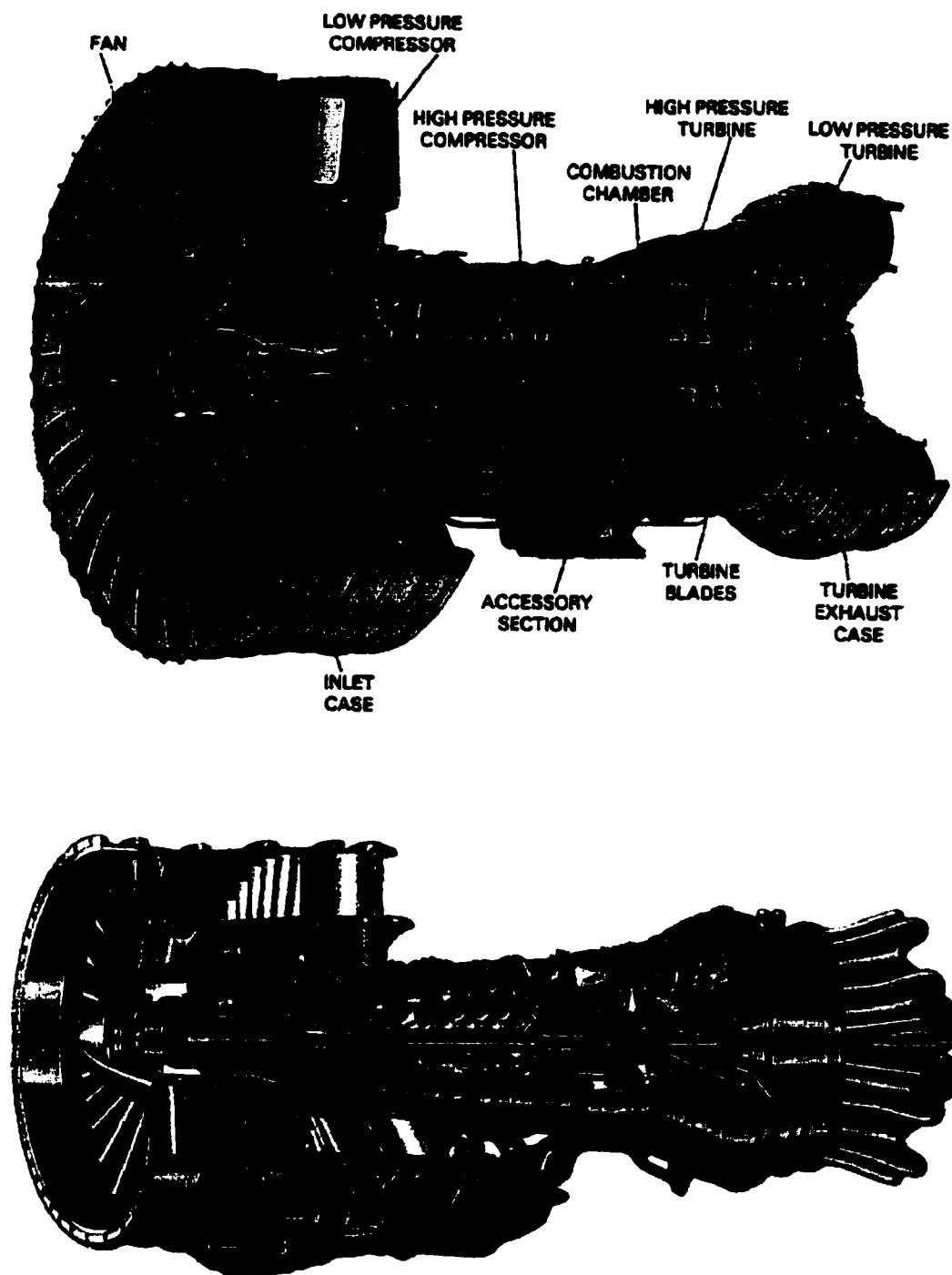


Figure 1-4 Large and mid size turbofan engines.

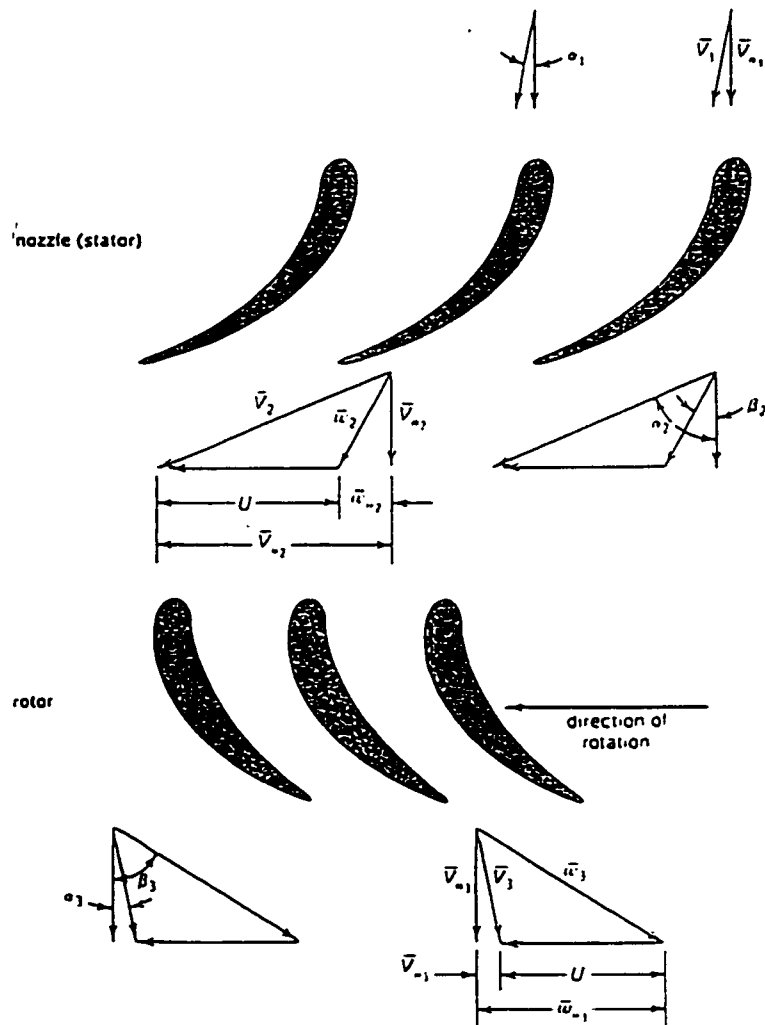
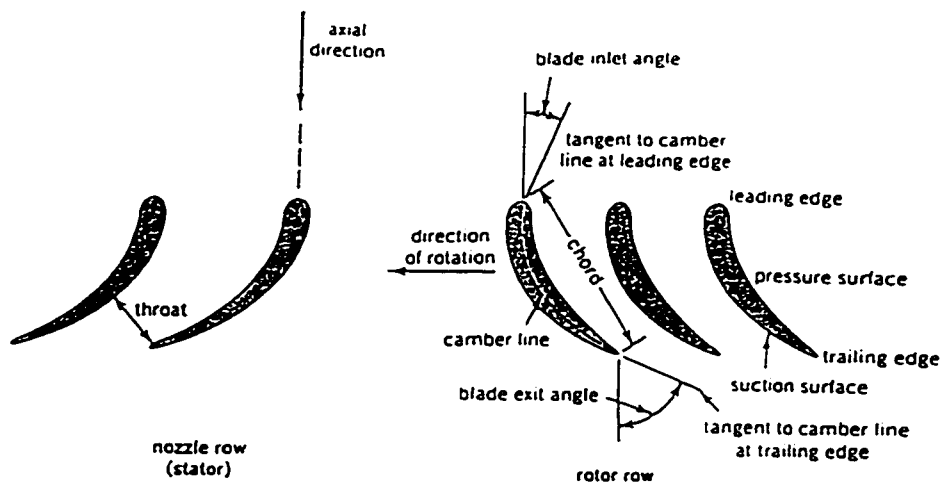


Figure 1-5 Axial turbine blade nomenclature and velocity triangle [4].

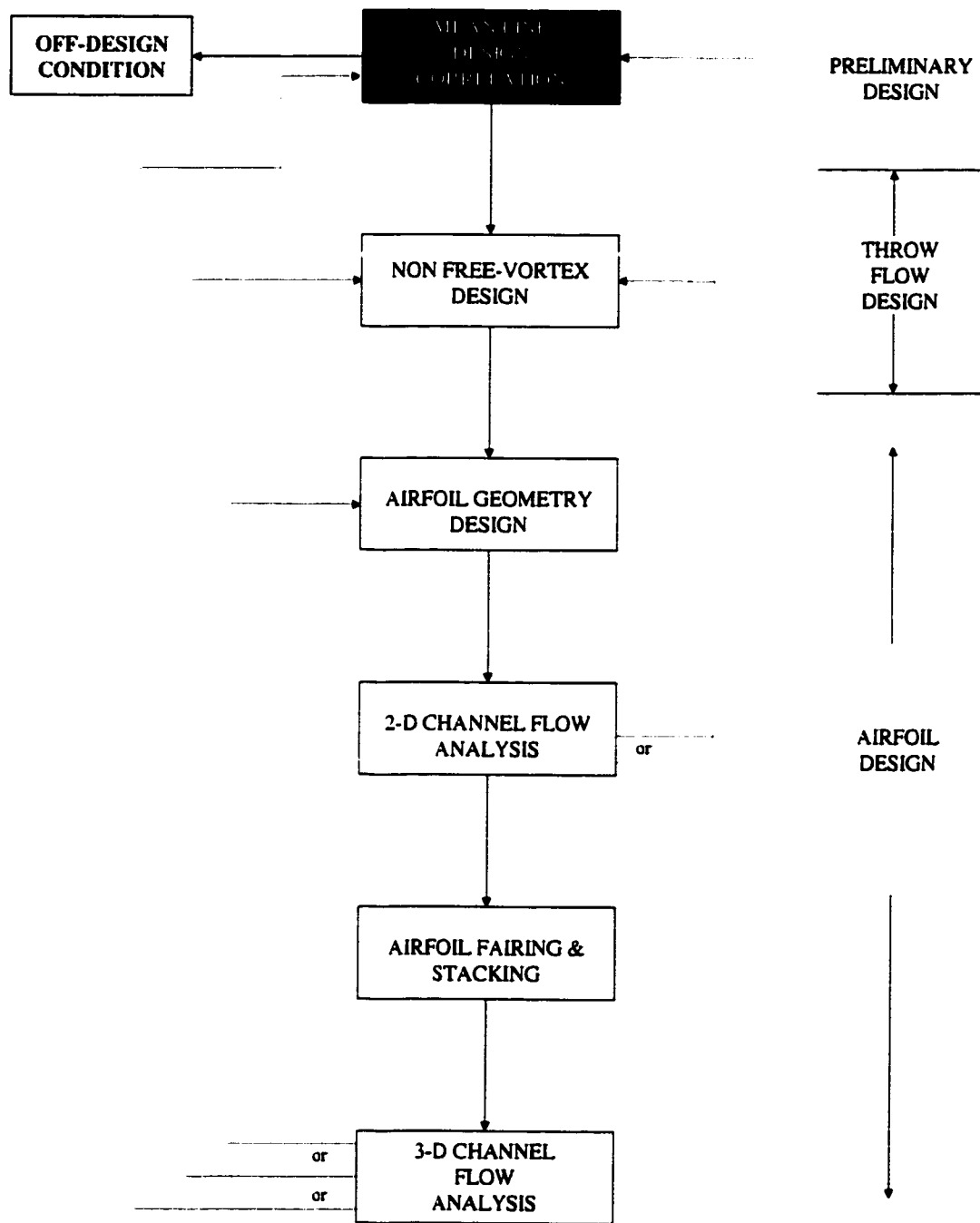


Figure 1-6 Aerodynamic design procedure for a gas turbine [38].

2. The test cases

The limited selection of the test cases was made to gauge the ability of a 3-D viscous flow analysis to reproduce the effect of some mean line design parameters and off-design parameters. The selection is based on the availability of experimental data, the ease of preparing the meshes and setting up the test cases, and most importantly, the usefulness of the chosen parameters to test the code and yield useful design correlations. In this chapter, the test cases will be outlined, the boundary conditions explained, and then, the CFD set-up and overview of the code will be given.

2.1. Outline of the test cases

Four parameters are selected in order to study their effects on the performance characteristics of a high-pressure turbine stage:

- Tip clearance/span
- Blade speed (rpm)
- Stage pressure ratio
- Vane stagger angle

The first test case is that of tip clearance. The tip clearance gap is varied over 3 different values: 0.5%, 1.5% (the design one) and 2.5% tip clearance/span. The performance characteristics of the turbine stage are compared with a fourth case that has no tip clearance. Also the important phenomenon of tip leakage vortex is studied.

The variation of the blade speed (rpm) is studied as the second test case. A wide range of blade speeds is studied. The speed is varied from 70% $(N/\sqrt{T})_{des}$ to 120% $(N/\sqrt{T})_{des}$, in intervals of 10% $(N/\sqrt{T})_{des}$. In this test case, a constant pressure ratio is maintained, so only the effect of the blade speed is analyzed.

As a third test case, the stage pressure ratio is varied at a constant blade speed. The range of pressure ratio studied is a large one, with the pressure ratio varied from 64 % PR_{des} to 121% PR_{des} .

A very interesting test case is chosen to conclude this work, namely the effect of vane stagger angle. The vane stagger angle is closed by only 0.8° for two different speeds: 70% $(N/\sqrt{T})_{des}$ and 100% $(N/\sqrt{T})_{des}$.

For all of the test cases performed, the results obtained from the flow solver are compared with experimental data and with the current turbine correlation model

at P&WC, except for the cases of blade tip clearance and vane stagger angle, since no experimental data were available for those test cases (from the tested turbine).

All comparisons to experimental data in this work are comparison to the data available from the P&WC Cold Flow Turbine Rig (CFTR) (see appendix A for blades and gas path geometry).

2.2. Description of the boundary conditions

Before explaining the boundary conditions, a description of the geometry and the stations used for the analysis is necessary. Figure 2.2-1 shows the actual geometry of the turbine stage and figure 2.2-2 the computational geometry of the vane and the blade. It is seen that the blade has a noticeably long downstream passage, due to the fact that the Inter-Turbine Duct (ITD) is included in the analysis. This is done because the experimental values have included the ITD in their calculations.

Figure 2.2-3 shows the location of the stations used in the analysis.

The turbine analysed in this work is a high-pressure transonic turbine, and it has the characteristics listed in Table 2.2-1. Using the parameters given in Table 2.2-1,

the boundary conditions are set in the code as follows (the features of the code will be explained in the next section):

- As an inlet to the stage (vane), a constant profile of $T_t = 770^\circ\text{R}$, $P_t = 14$ psia, $M = 0.15$ and $\alpha = 0^\circ$ are imposed.
- At the exit plane of the stage (blade), static pressure $p = 2.925$ psia is imposed.

This value of $p_{4a} = 2.925$ psia is derived as follows:

Since $PR = \frac{P_{t1}}{P_{t4a}} = 4.04$ and $P_{t1} = 14$ psia $\Rightarrow P_{t4a}$ is obtained to be 3.47 psia. Since

$M_{4a} = 0.5$, p_{4a} is found using:

$$\frac{P_t}{p} = \left(1 + \frac{\gamma - 1}{2} M^2 \right)^{\frac{\gamma}{\gamma - 1}} \quad (2.2-1)$$

For the test cases involving changes of the blade speed, this value (p_{4a}) has to be changed by trial and error in order to get a constant stage PR. Due to the fact that the experimental data are obtained from a CFTR that has been run at a relatively low temperature, and assuming ISA (here air is the working fluid), the value of gamma used in the above equation (2.2-1) is assumed to be 1.4. The mass flow of the stage is set to be $2.51 \text{ lb}_m/\text{s}$, as obtained from $m\sqrt{T_t}/P_t$ (Table 2.2-1). The blade speed (N) is obtained from the relation $N/\sqrt{T_{t1}} = 668$ (Table 2.2-1) and it is equal to 18536 rpm.

In order to simplify the physics of the problem, no cooling is considered, and thus, all walls are set to be adiabatic. In the analysis presented in this work, the efficiency is calculated using the following equation:

$$\eta = \frac{T_{t1} - T_{t4}}{\left(T_{t1} - \left(\frac{P_{t4}}{P_{t1}} \right)^{\frac{\gamma-1}{\gamma}} \right)} \quad (2.2-2)$$

The value of gamma used here is calculated based on the averaged in and out temperature (T_{t1} and T_{t4}), since here the two temperatures are available from the CFD code at this point. It can be seen from this equation (2.2-2), that the ITD is also included in the calculation of the efficiency. This is because, as mentioned earlier, the experimental values available include the ITD. As it can also be seen from figure 2.2-3 and the above equation, the efficiency is calculated down to the “Measuring Plane” (station 4), and not to the exit plane (station 4a). This is because station 4 is the plane at which the experimental measurements were taken. The small extension from station 4 to station 4a was suggested to be added so that the exit boundary conditions would not be forced at the plane where the experimental data was collected.

The aerodynamic loss of each component is calculated using:

$$\Delta P / P = DELP / P = \frac{P_{t_{in}} - P_{t_{out}}}{P_{t_{in}}} \quad (2.2-3)$$

The stage reaction (the ratio of the drop of static pressure across the blade to that of the stage) is calculated using the following equation:

$$R = \frac{p_2 - p_3}{p_1 - p_3} \quad (2.2-4)$$

In the detailed analysis tables that will be presented later (in Chapter 3), each component is studied separately (vane, blade and ITD). Thus, specific planes, which are close to the components (vane and blade), were chosen. Certainly, there is still some questions about which plane (inlet, ..., LE-10% chord, LE-5% chord, LE, TE, TE+5% chord, TE+10% chord, ..., exit) is the appropriate one to be chosen; and whether it takes into account the mixing losses or not [39,47,48]. Despite the many published papers about this topic, no specific plane has been found to be the ideal one. In our analysis, the planes: LE-10% chord and TE+10% chord were chosen in consultation with gas turbine designers.

The results of the turbine correlation were obtained using a P&WC in-house code, which is based on the modified AMDC (see section 1.1) loss system [41], and with some improvements such as those described in reference [55].

In the next section, an overview of the features of the 3-D viscous code (*NS3D*) used will be highlighted, and the CFD set-up will be explained.

2.3. CFD set-up and overview of the NS3D code

A hexahedral, structured, grid is used. All the test cases use the same mesh except the tip clearance test cases, since the tip clearance is variable. Despite this, the number of nodes and the number of elements are the same. Table 2.3-1 shows a summary of the meshes used. As it can be seen, three meshes are used, one for each of the vane, the blade and the blade tip regions. A presentation of the meshes used is made in figure 2.3-1 & 2.3-2.

The 3-D viscous, compressible code used (*NS3D*) solves the three-dimensional, Reynolds-averaged, Navier-Stokes equations. The steady version of the code is used with a (κ - ω) turbulent model. *NS3D* has the following features (see figure 2.3-4 for the flow chart of the complete CFD analysis) [50]:

- Galerkin finite element discretization
- Equal order interpolation for velocity and pressure terms, stabilised through an explicit pressure dissipation & streamline upwinding
- Newton linearization with fully-coupled solution of the velocity vector and the pressure
- Turbulent (the turbulence model used is κ - ω)
- Large-scale iterative solvers parallelized for distributed memory architectures (ILU-PCG)

- Near-wall region solved using a wall integration through a "logarithmic" element
- Mixing plane between components (figure 2.3-3): the interface between the components (vane and blade) has a mixed boundary condition. The upstream interface plane is treated as an exit of the previous blade row, whereas the downstream interface plane is treated as an inlet to the following blade row. Boundary conditions are continually interchanged at such planes as are updated iteratively by the flow solver.

Solution Procedure for mixing plane method is:

- Solve each blade row with inlet and exit boundary conditions
- Iteratively update boundary conditions at the mixing plane via proper averaging methods
- Match radial profiles or averaged flow properties at the mixing plane

Mesh Requirements for mixing plane method are:

- Single passage mesh for each blade row with tip clearance
- Non overlapping grids between blade rows
- Mixing plane shared between adjacent blade rows normal to engine axis
- Identical spanwise grid point distribution at the mixing plane (is strongly recommended).

The derivation of thermodynamic variables is based on a "mixed-out" approach, which assumes that the flow is instantly mixed at the mixing plane [50].

BC's (section 2.2)

P.R.	4.04	Vane count	15
$\Delta H/U^2$	1.83	Blade count	70
Cx/U	0.64	Vane aspect ratio	0.5
Inlet total pressure (psi)	14	Blade aspect ratio	2
Inlet total temperature (°R)	770	Vane % TE blockage	6.8
Inlet Mach number	0.15	Blade % TE blockage	9.3
Exit Mach number	0.5	Clearance/span (%)	1.5
Exit swirl (degrees)	16.8	α_1 (degrees)	0
$m\sqrt{Tt1}/Pt1$	4.98	η (%)	84.5
$N/\sqrt{Tt1}$	668		
Blade $Re \times 10^{-3}$	63		
$AN^2 \times 10^{-10}$	7.9		

Table 2.2-1 Turbine stage characteristics and boundary conditions.

CFD meshes (section 2.3)

	Vane	Blade	Blade Tip	Total
Total number of I plane	125	145	49	319
L.E. at I plane	43	27		-
T.E. at I plane	91	75		-
Total number of J plane	27	27	5	59
Total number of K plane	35	30	6	71
Total number of nodes	118125	137025	1470	256620

Table 2.3-1 Mesh details.

Turbine geometry & Analysis stations location (section 2.2)

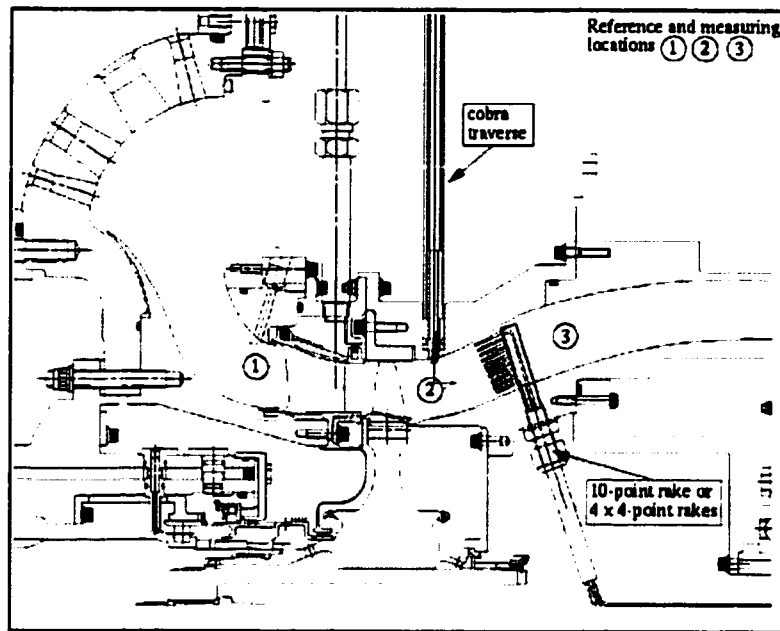


Figure 2.2-1 Turbine stage actual geometry[60].

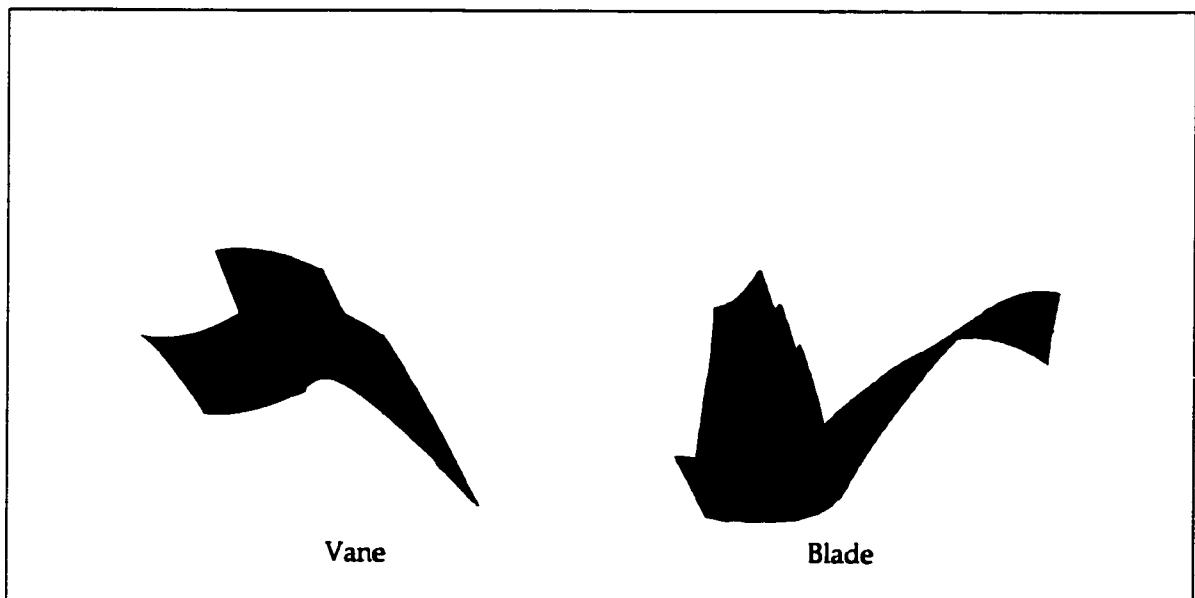


Figure 2.2-2 Vane and Blade geometry.

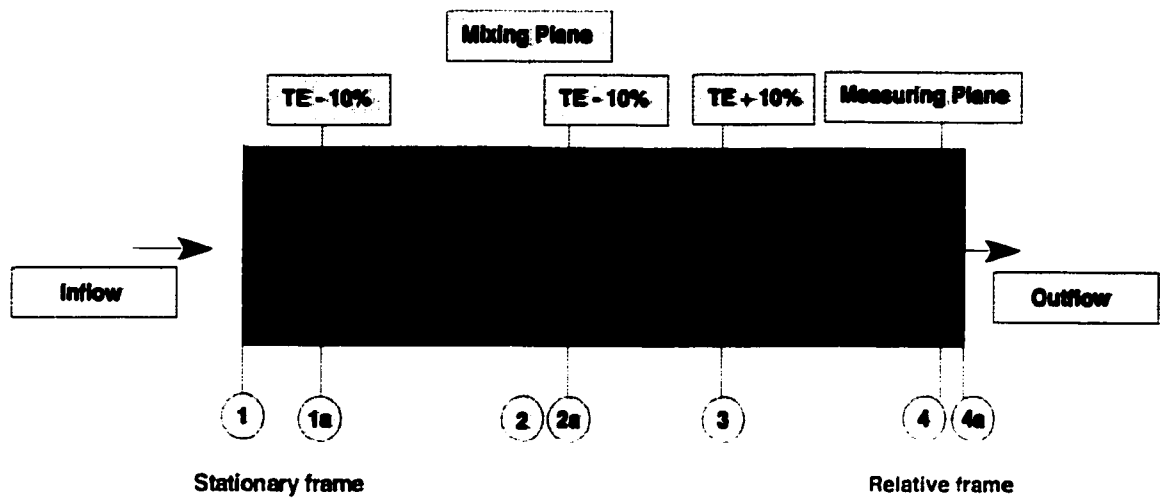


Figure 2.2-3 Location of analysis stations.

CFD meshes (section 2.3)

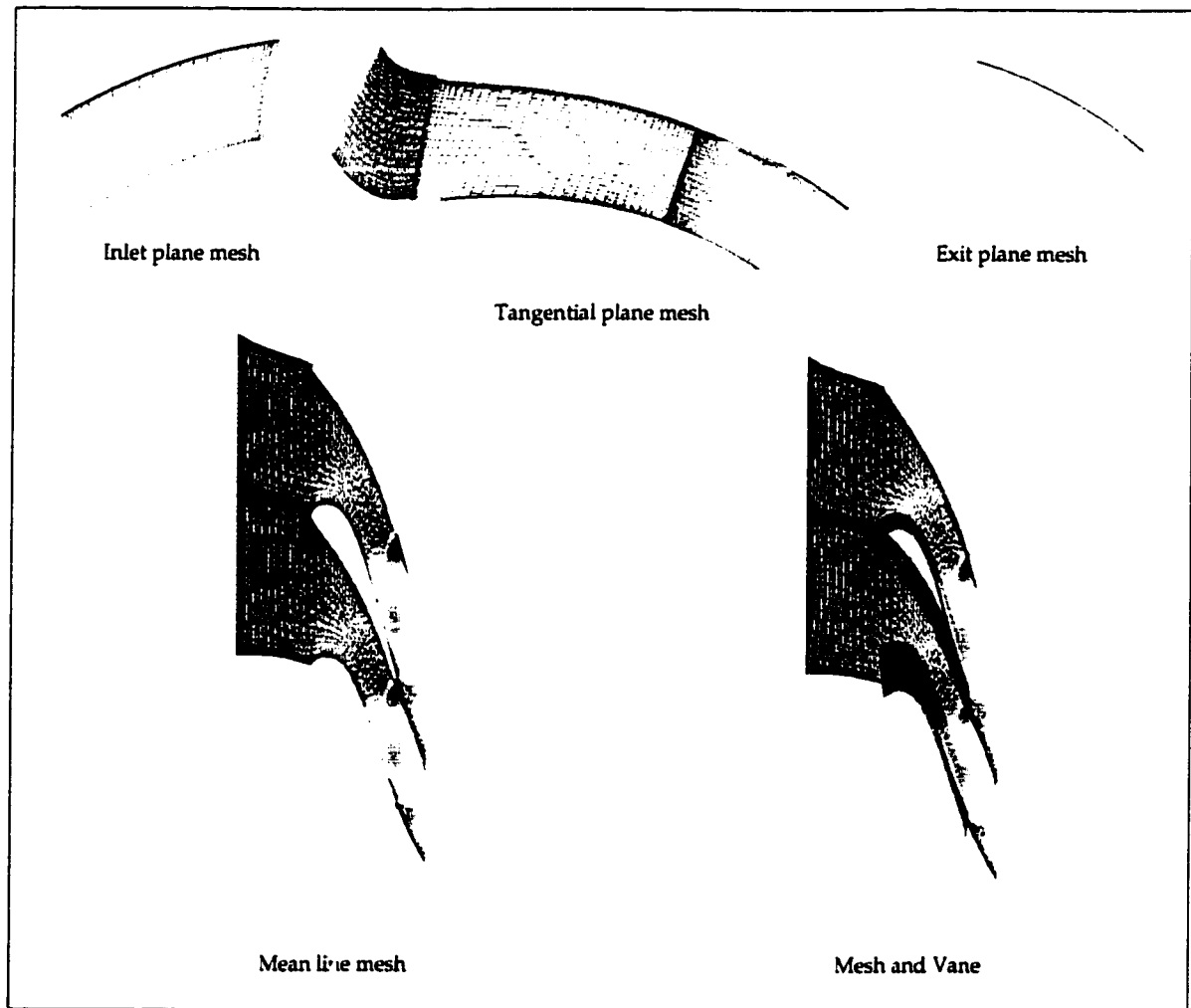


Figure 2.3-1 Vane computational mesh (here colour does not have any physical meaning).

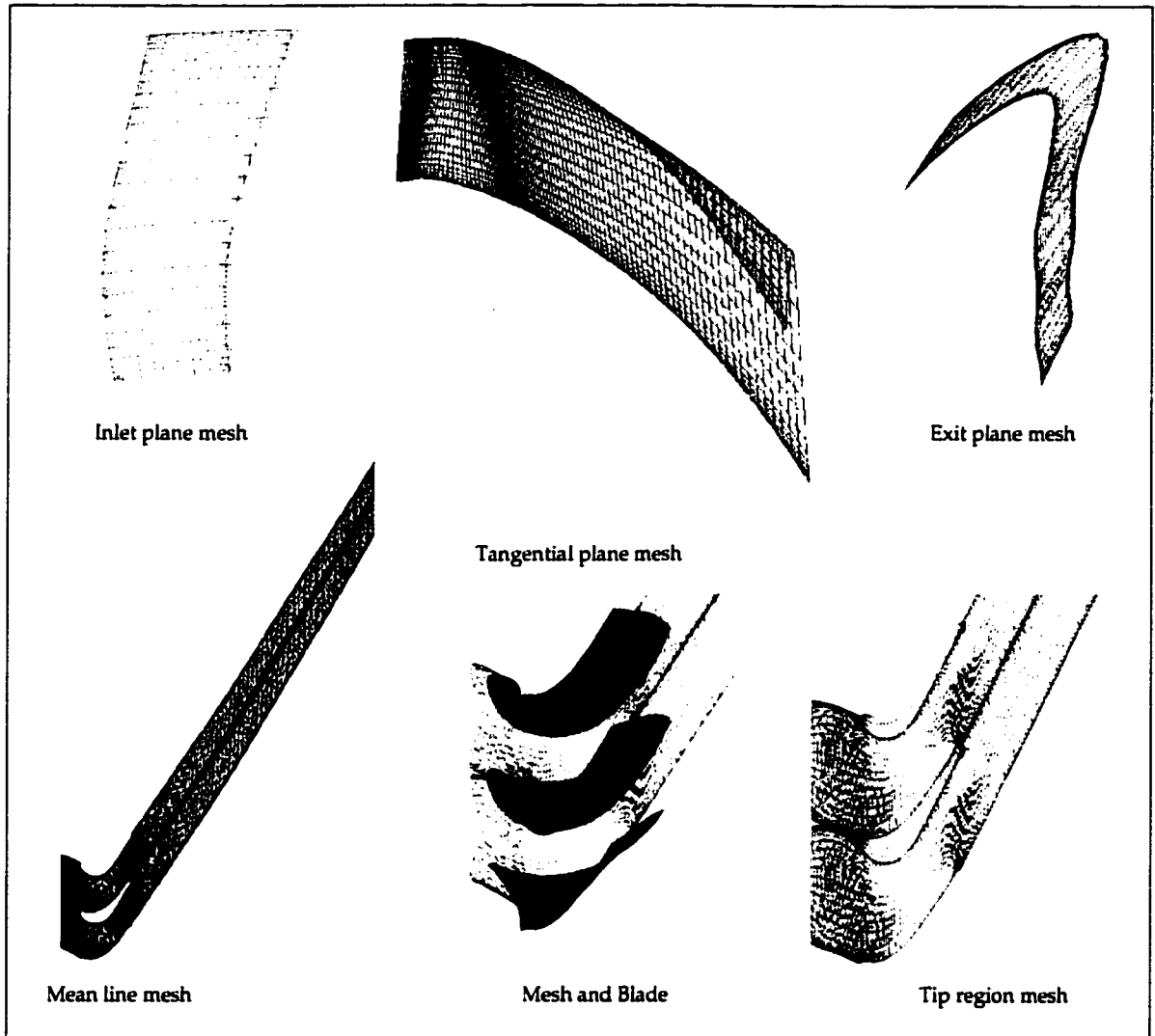


Figure 2.3-2 Blade computational mesh (here colour does not have any physical meaning).

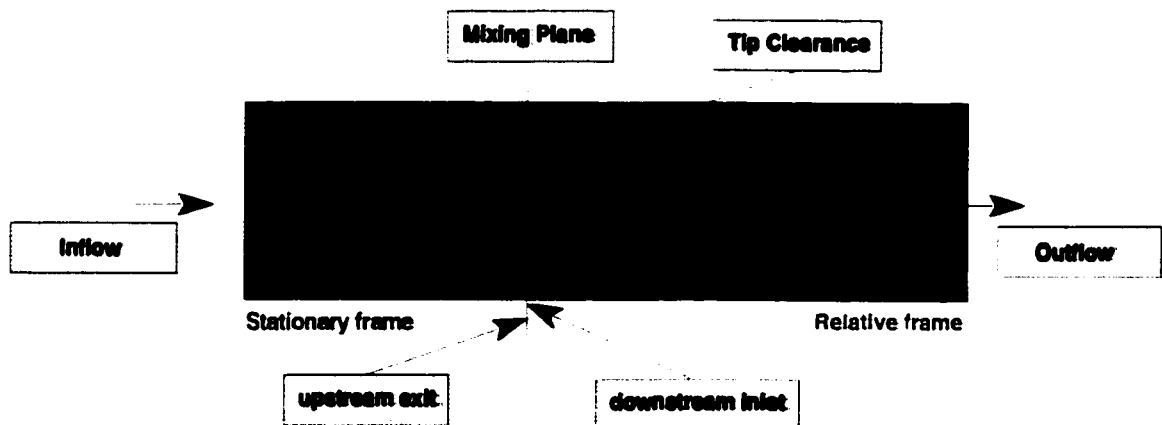


Figure 2.3-3 Regions descriptions [50].

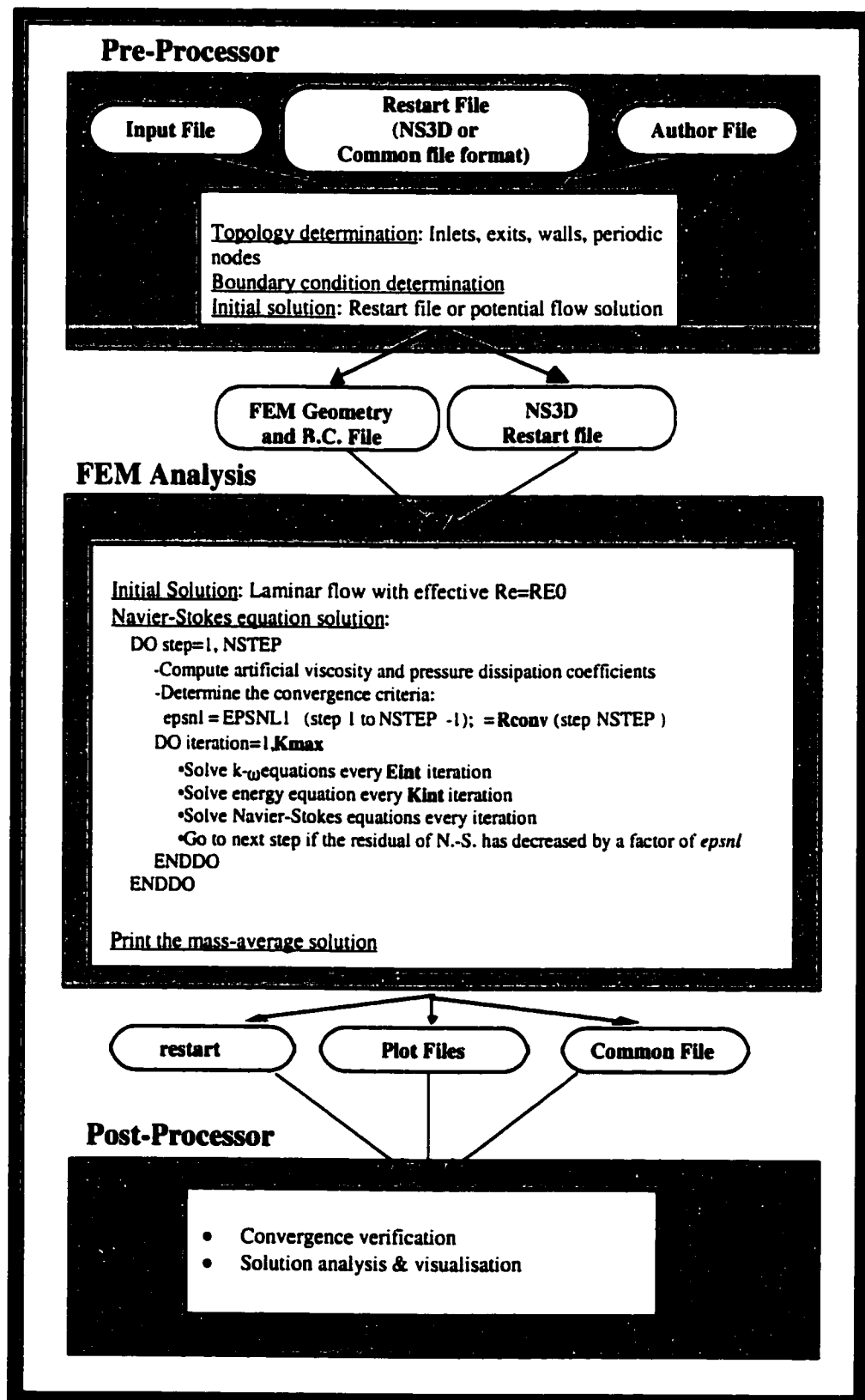


Figure 2.3-4 CFD analysis procedures [50].

3. Parameters studied

3.1. Effect of Tip Clearance (clearance/span) on performance characteristics of high-pressure turbine stage

Understanding the flow structure through the tip gap of axial flow turbomachinery blade rows is very important, since it has interrelated adverse effects on the performance of the engine. The losses associated with the leakage flow account for a significant fraction of the losses in the endwall region. Also, leakage alters the blade loading in the tip region and thus affects the flow turning ability of the blade.

NS3D is used to analyze the effect of changing tip clearance on the performance of the HPT. Figure 3.1-1 plots the variation of turbine stage efficiency versus % blade tip clearance/span (Table 3.1-1). The results of *NS3D* and turbine correlation are shown (as mentioned earlier, for this test case, no test results are available from the CFTR). It is noticed that *NS3D* compares reasonably well with the mean line results. Both curves agree on the fact that, a significant decrease in efficiency results from any increase of the tip clearance for the range shown.

Figure 3.1-2 represents *NS3D* predictions for vane mid span Mach number distribution. It shows that the change of the size of the tip clearance gap has no

significant effect on the loading of the vane in the mid span region. This is also the case for the vane loading in the tip region, as can be seen in figure 3.1-3. Figure 3.1-4a shows that as the tip clearance increases, the blade loading at the LE area increases, whereas it decreases at the TE area.

To examine the effect of the tip leakage vortex on the blade loading, the blade surface Mach number distribution is plotted at different regions close to the tip in figure 3.1-4. From this figure, it is clearly noticed that the no tip clearance case has practically no change in loading, whereas the other cases show an overall increase in loading. More specifically, the loading moves toward the TE, but no common behaviour was found. This is probably due to the fact that the size, the strength and the number of the tip leakage vortices are different from one case to another [3].

In order to understand the characteristics of the tip leakage vortex, the power of the CFD tool is put to the test. Figure 3.1-5 shows the simulation of the tip leakage vortex for the three tip clearances tested. As expected, a good examination of the figures confirms the fact that as the tip clearance gap increases, the vortex becomes bigger and stronger [3,47].

Further investigations on the behavior of the tip leakage vortex will be done in the next section, but for now, the influence of the size of the tip clearance gap is

analyzed using Table 3.1-2. This table shows that as the tip clearance is increased the exit relative swirl from the blade decreases, and thus, the turning ability of the blade is reduced.

Table 3.1-2 reveals that for the 2.5% tpclr case, the ITD has relatively high losses (DELP/P in the Table) compared to the other cases. This is believed to be caused by the relatively stronger and bigger tip leakage vortex, and thus, as will be seen in the next section, the vortex does not get diffused until practically the end of the duct (around 3.47 blade chords downstream from the blade TE).

The degree of reaction of the turbine stage is calculated and shown for different tip clearances in figure 3.1-6 and Table 3.1-3. It is noticed that while no significant change is found in the stage reaction for the four tip clearances modeled, a relatively lower reaction is found for the 2.5% tpclr case.

Tip Clearance (section 3.1)

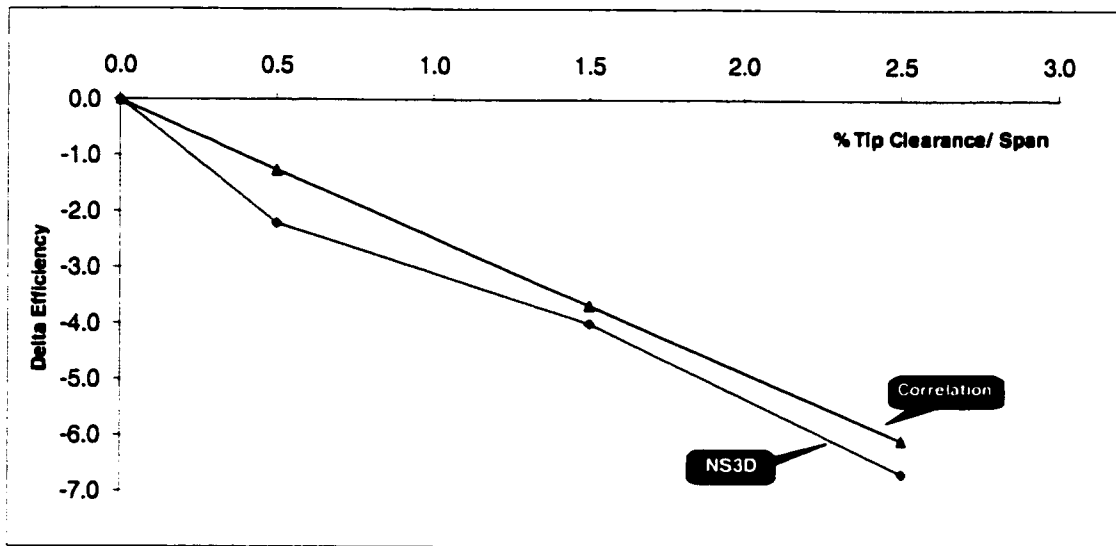


Figure 3.1-1 NS3D predictions for the variation of stage efficiency vs. blade tip clearance.

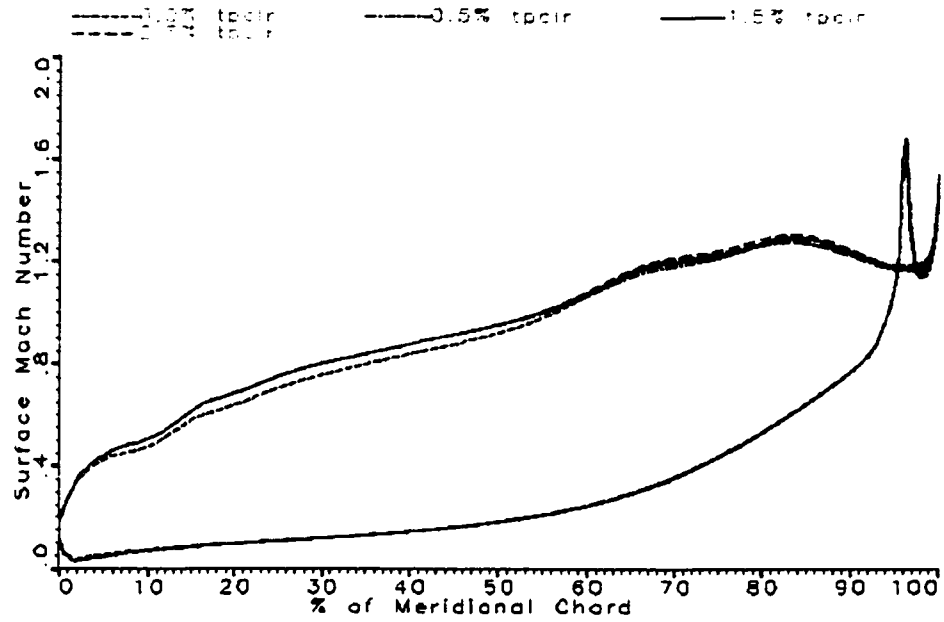


Figure 3.1-2 NS3D predictions for vane mid-span Mach number distribution, for all the tip clearances.

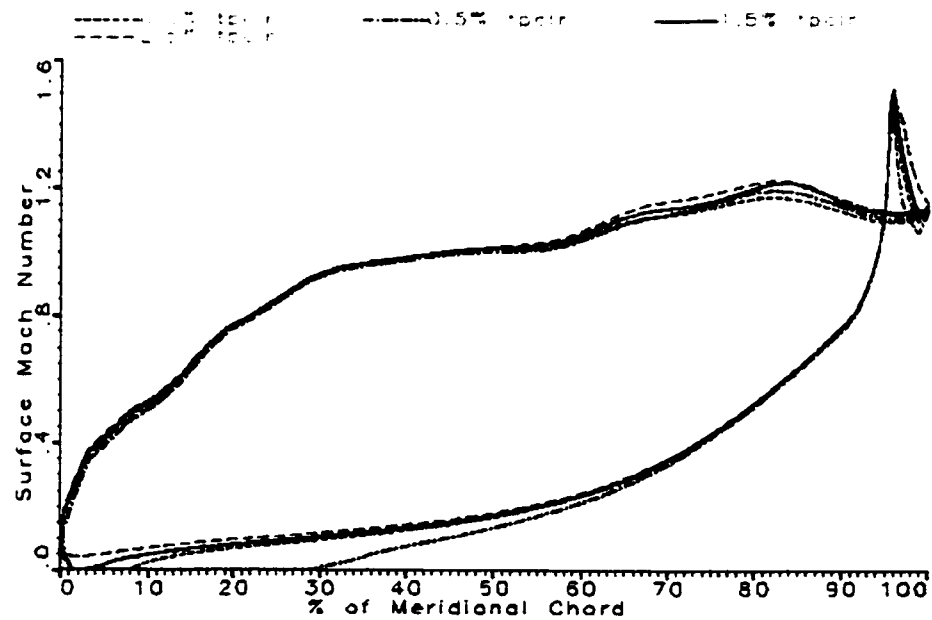
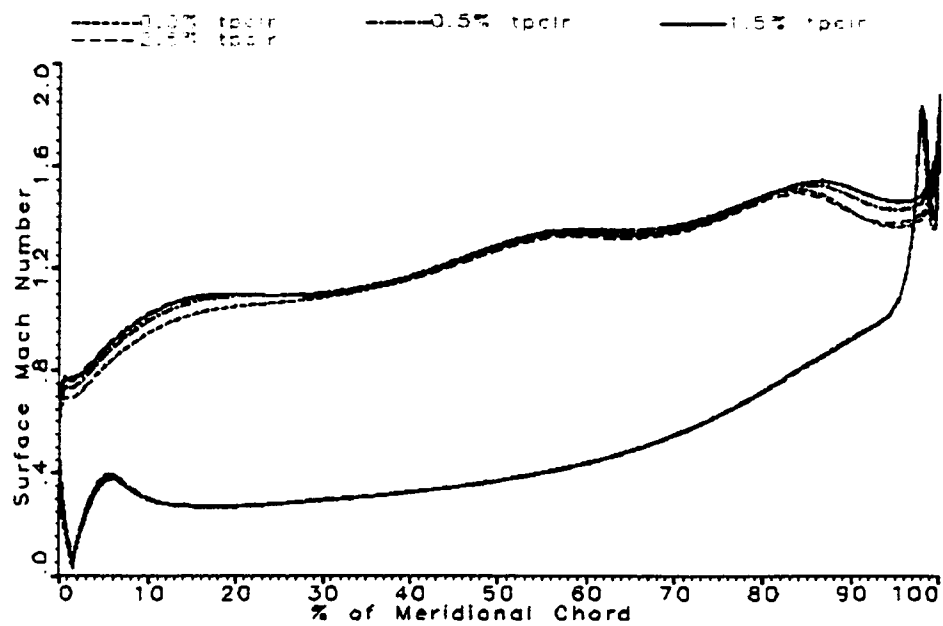
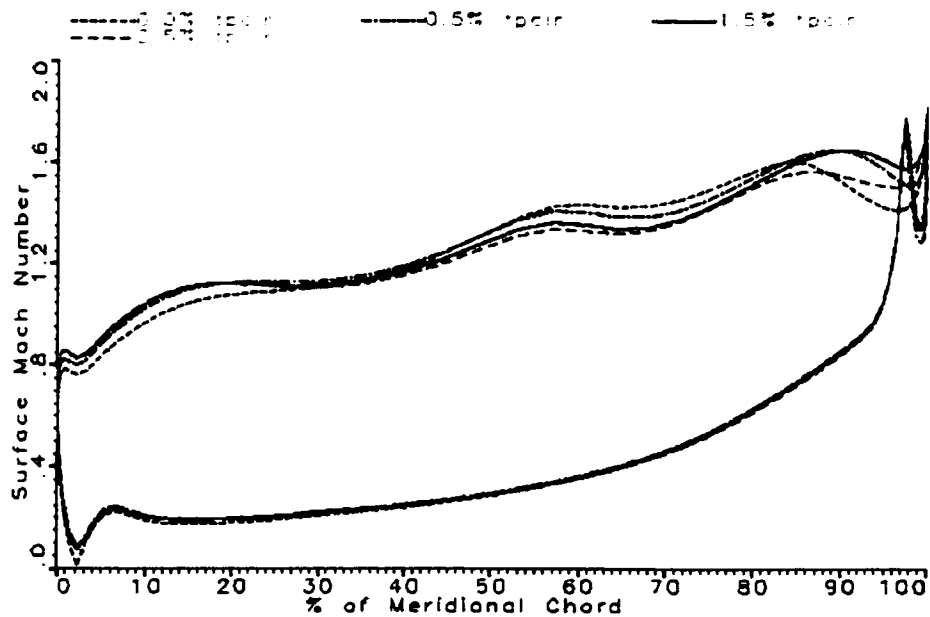


Figure 3.1-3 NS3D predictions for vane Mach number distribution at 99% span, for all the tip clearances.

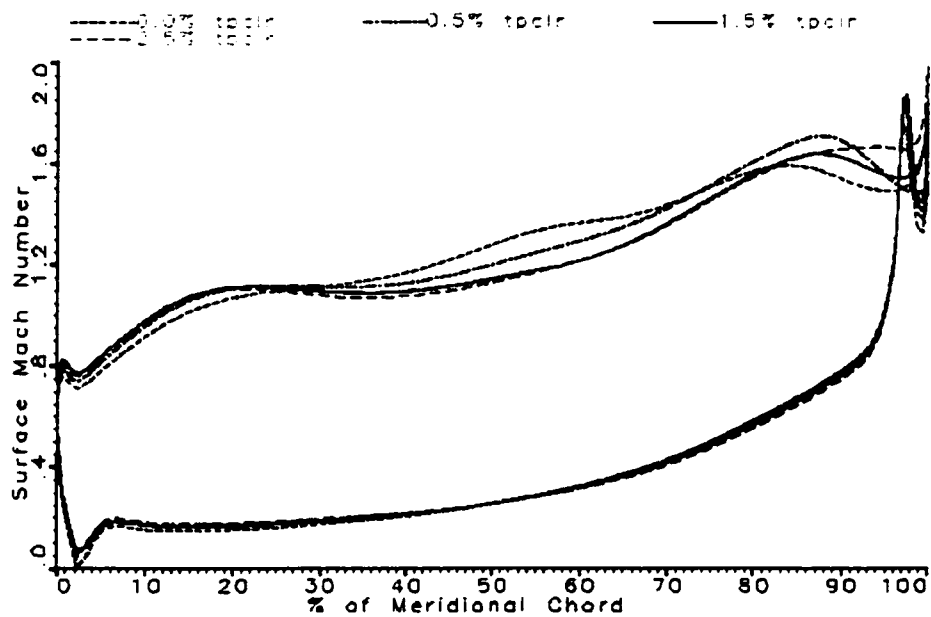


(a) Blade loading at mid span

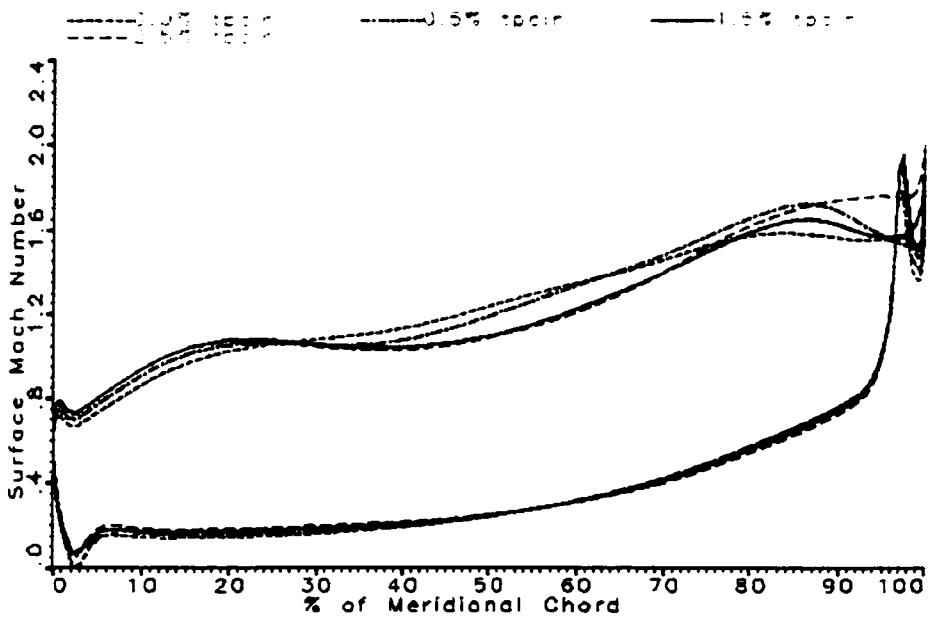


(b) Blade loading at 75% span

Figure 3.1-4 NS3D predictions for blade Mach number distribution at different span locations, for all the tip clearances.

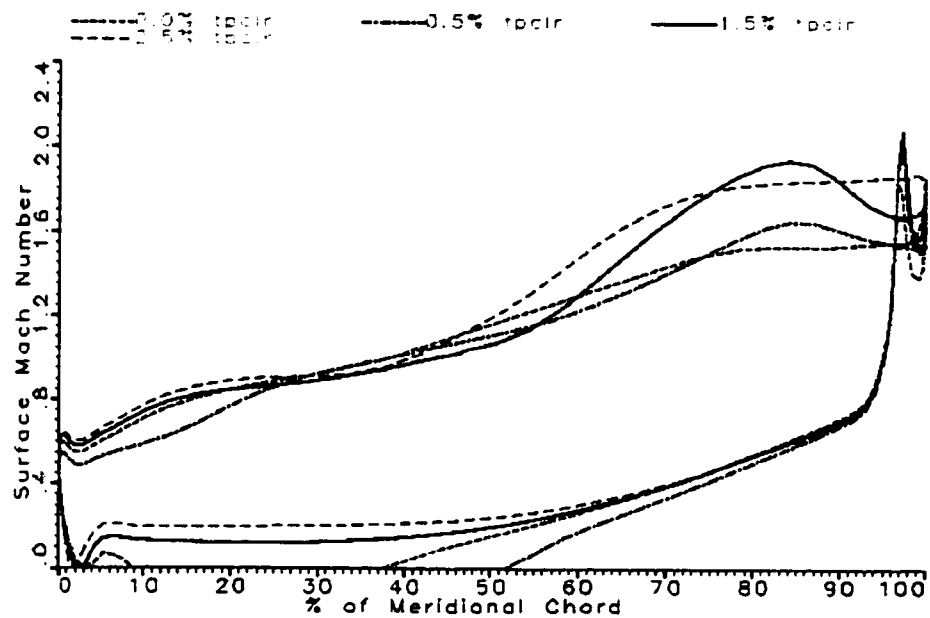


(c) Blade loading at 86% span

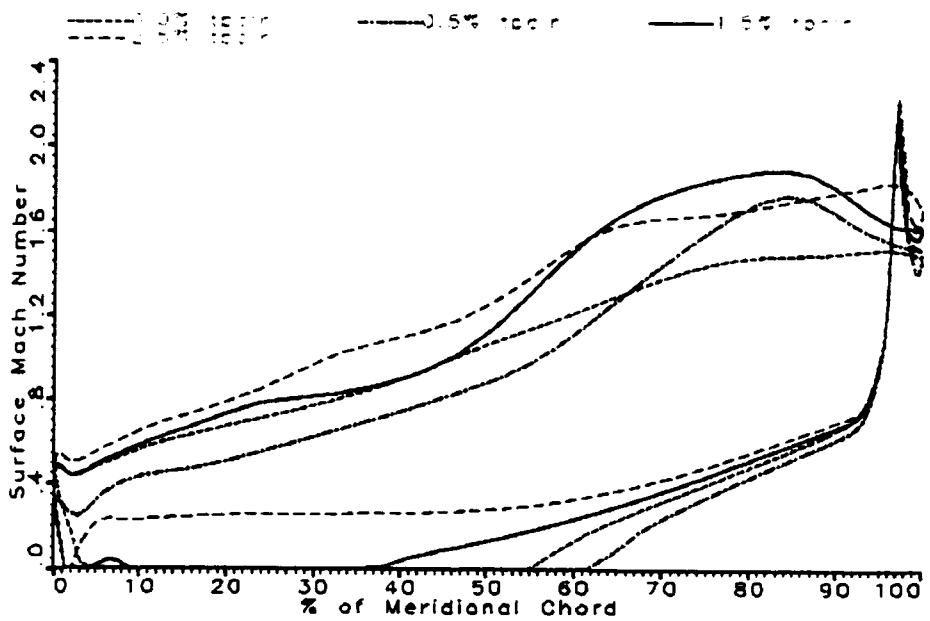


(d) Blade loading at 90% span

Figure 3.1-4 (suite) NS3D predictions for blade Mach number distribution at different span locations, for all the tip clearances.



(e) Blade loading at 96% span



(f) Blade loading at 98% span

Figure 3.1-4 (suite) NS3D predictions for blade Mach number distribution at different span locations, for all the tip clearances.

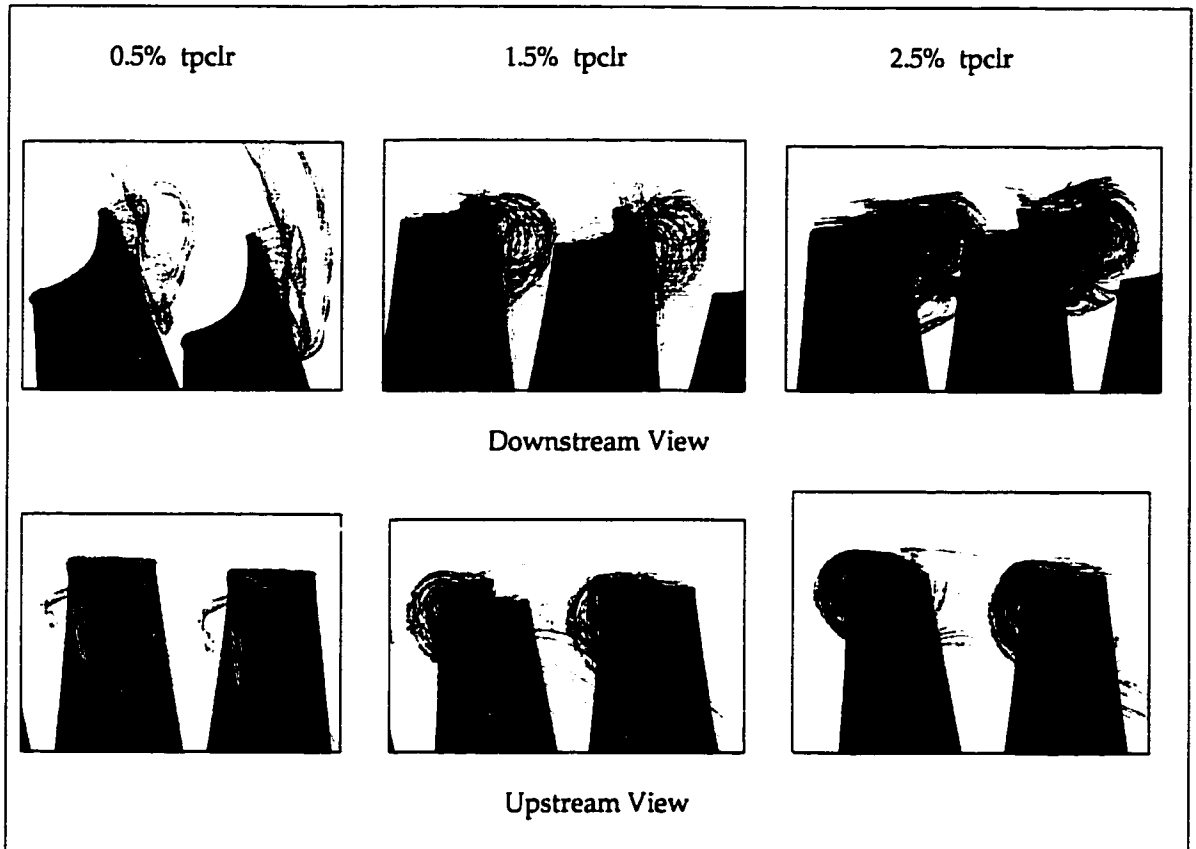


Figure 3.1-5 Views of the tip leakage vortex for the three blade tip clearances as predicted by NS3D.

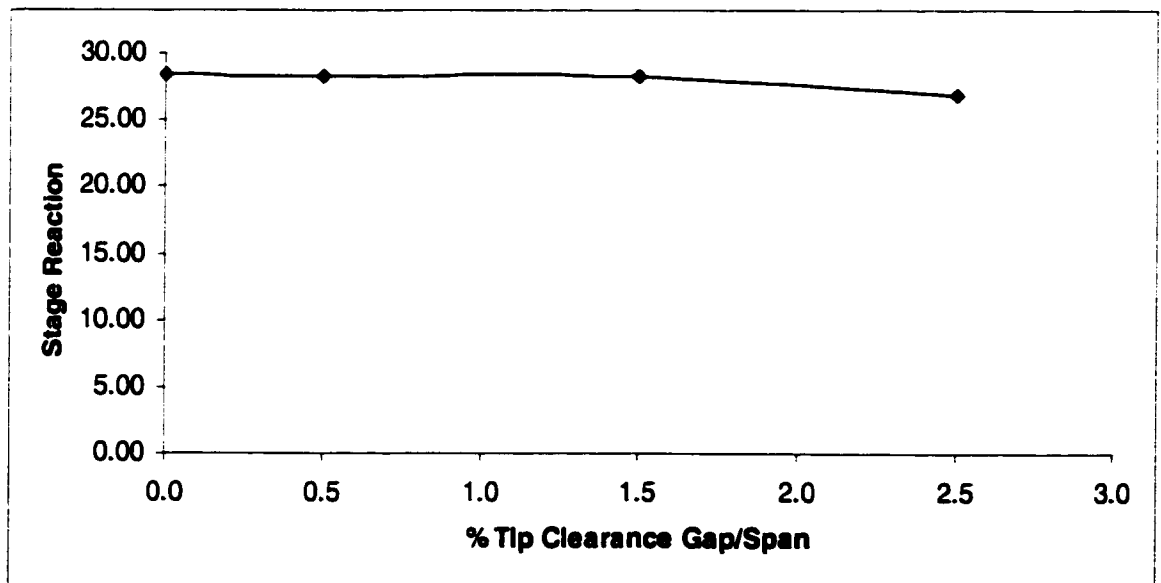


Figure 3.1-6 NS3D predictions for averaged stage reaction, for all the tip clearances.

Tip Clearance (section 3.1)

	0.0 % tpcir	0.5 % tpcir
Pt1	13.9980	13.9980
Pt4	3.5134	3.3651
Tt1	770.0000	770.0000
Tt4	547.2945	546.6831
$T_{avg} = (Tt1 + Tt4)/2$	658.6473	658.3416
Gamma(T_{avg})	1.3975	1.3976
ETA(effic. %)	88.987	86.997
% ETA diff. from 0.0%tpcir	0.00	-2.21

Table 3.1-1 Stage efficiency of the four blade tip clearances.

	0.0 % tpcir	0.5 % tpcir
Vane: From -10% LE to GAP COMP AVERAGED DOWNSTREAM		
Pt1a	13.9772	13.9772
Pt2	12.8870	12.9866
DELP/P	0.0780	0.0709
M2	1.1262	1.1518
Blade: From -10% LE to +10% TE		
Swirl(r)2a	48.0385	48.9021
Delta Swirl2a from Design	-2.5503	-1.6868
Ptr2a	6.9323	6.8573
Ptr3	6.3501	6.2073
DELP/P	0.0840	0.0948
Mr3	1.1730	1.2070
M3	0.8577	0.7024
Swirl(r)3	58.9712	57.6148
Duct: From +10% TE to measuring plane		
Pt3	3.6310	3.5308
Pt4	3.5134	3.3651
DELP/P	0.0324	0.0469
Mr4	1.1585	1.1593
M4	0.5262	0.5438
Swirl(r)4	66.1881	64.6448
Swirl4	24.3500	26.8200

Table 3.1-2 Stage detailed analysis for all the tip clearances studied.

	0.0 % tpcir	0.5 % tpcir
P1	13.7810	13.7810
P2	5.8577	5.7148
P3	2.7186	2.5439
R (%)	28.3682	28.2160
% R from R(des)	0.3502	-0.1918

Table 3.1-3 Influence of blade tip clearance on the stage reaction.

3.1.1 Tip Leakage Vortex

Despite the fact that experimental data is very important to validate the flow solver used to compute the flow field, it is often not detailed enough to give a complete description of the flow, because of the complex flow structure and blade geometry [19]. Thus, a CFD tool will be extremely useful for such analysis. A good example of complex flow phenomena is the tip leakage vortex of a turbine blade.

In order to understand the behavior of the tip leakage vortex in detail, the test case with the largest tip clearance (2.5 % tip clearance/span) is chosen, because multiple tip leakage vortices are expected. Also, since the vortices were found to be bigger than the other test cases, they are easier to study.

Figure 3.1.1-1 plots the predicted blade loading at different spans for the 2.5 % tpclr. As it has been found in the previous section, the loading of the blade moves from the LE to TE, as we get closer to the blade tip, and the overall loading slightly increases. This is due to the fact that the tip leakage vortex is more developed and stronger as we move toward the TE, and thus, causing higher pressure difference between the suction and pressure sides of the blade.

The possibility of finding multiple tip leakage vortices is conducted using FieldView (post-processing software), with animations done, and some interesting results found.

Figure 3.1.1-2 shows the static pressure contour lines at three different planes (A, B & C). At plane A (figure 3.1.1-2a), the first vortex is found, whereas at plane B (figure 3.1.1-2b), two vortices are detected. A third vortex is found to take shape at plane C (figure 3.1.1-2c). This last vortex does not, however, seem to be strong enough, because, as it will be seen later, it gets merged with the second vortex and only two distinct vortices remain at the TE + 0.16% chord plane.

Figure 3.1.1-3 shows a 3-D velocity vector presentation at the three planes in question. Unfortunately, due to the fact that the mesh used is relatively coarse for this kind of analysis, it was not possible to see all three expected vortices. The main and big vortex (the first one) is observed and it can be seen that the vortex is first located just under the blade tip, attached to the suction side (plane A & B), and then, starts to get detached from the blade (plane C).

To verify further the findings of multiple vortices, Mach number contours (based on relative velocity) and entropy contour lines were plotted in figure 3.1.1-4 & 3.1.1-5. A good examination of the figures lead to the same conclusion, and in fact, three vortices are seen. This finding confirms what Amrud and Sjolander

(1986) [3] found about the formation of multiple tip leakage vortices at larger clearances.

Further analysis on the behavior of these vortices was performed using some animation. Entropy contour lines and distribution are shown in figure 3.1.1-6 and show that at 0.16 blade chord from the TE (plane D), only two vortices were found, which in turn get merged into a single large and strong vortex at around 0.41 blade chord downstream of the blade TE (plane E).

In order to follow the evolution of the vortex across the ITD, the entropy distribution and contour lines were plotted at different planes in figures 3.1.1-7 & 3.1.1-8. By examining these plots (and with the help of some animations) the vortex is found to be completely diffused close to the exit of the duct at plane J (TE + 3.47 chord). It is also found that the center of the vortex moves practically parallel to the tip wall and away from the suction side toward the pressure side as one moves downstream.

Tip Leakage Vortex (section 3.1.1)

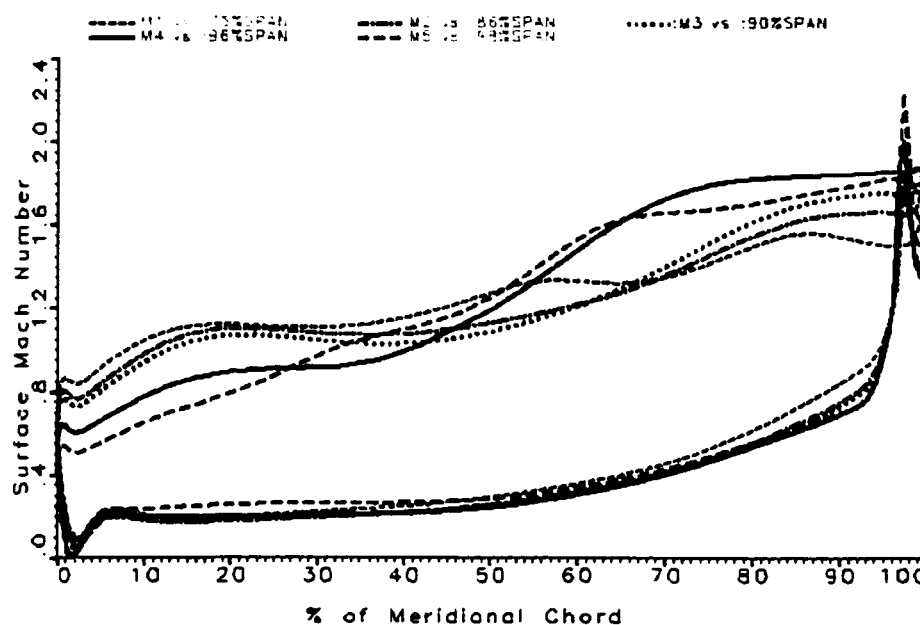


Figure 3.1.1-1 NS3D predictions for the 2.5% tip clearance/span blade Mach number distribution at different span locations.

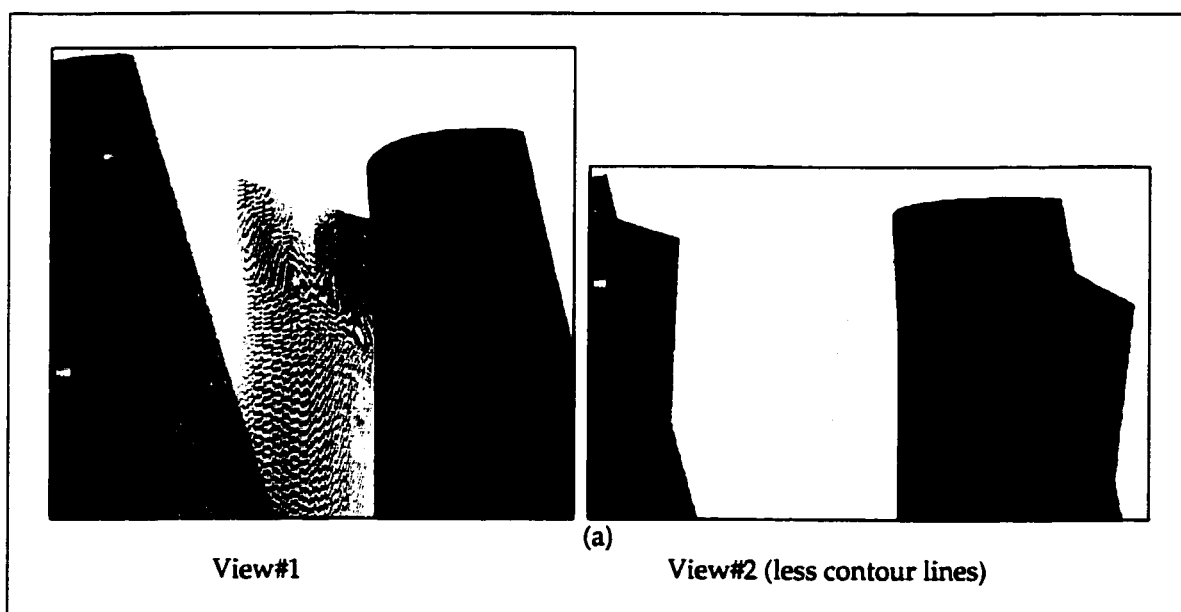


Figure 3.1.1-2 Static pressure contour lines: (a) at plane A (45.55% chord), (b) at plane B (50.70% chord), (c) at plane C (99.50% chord).

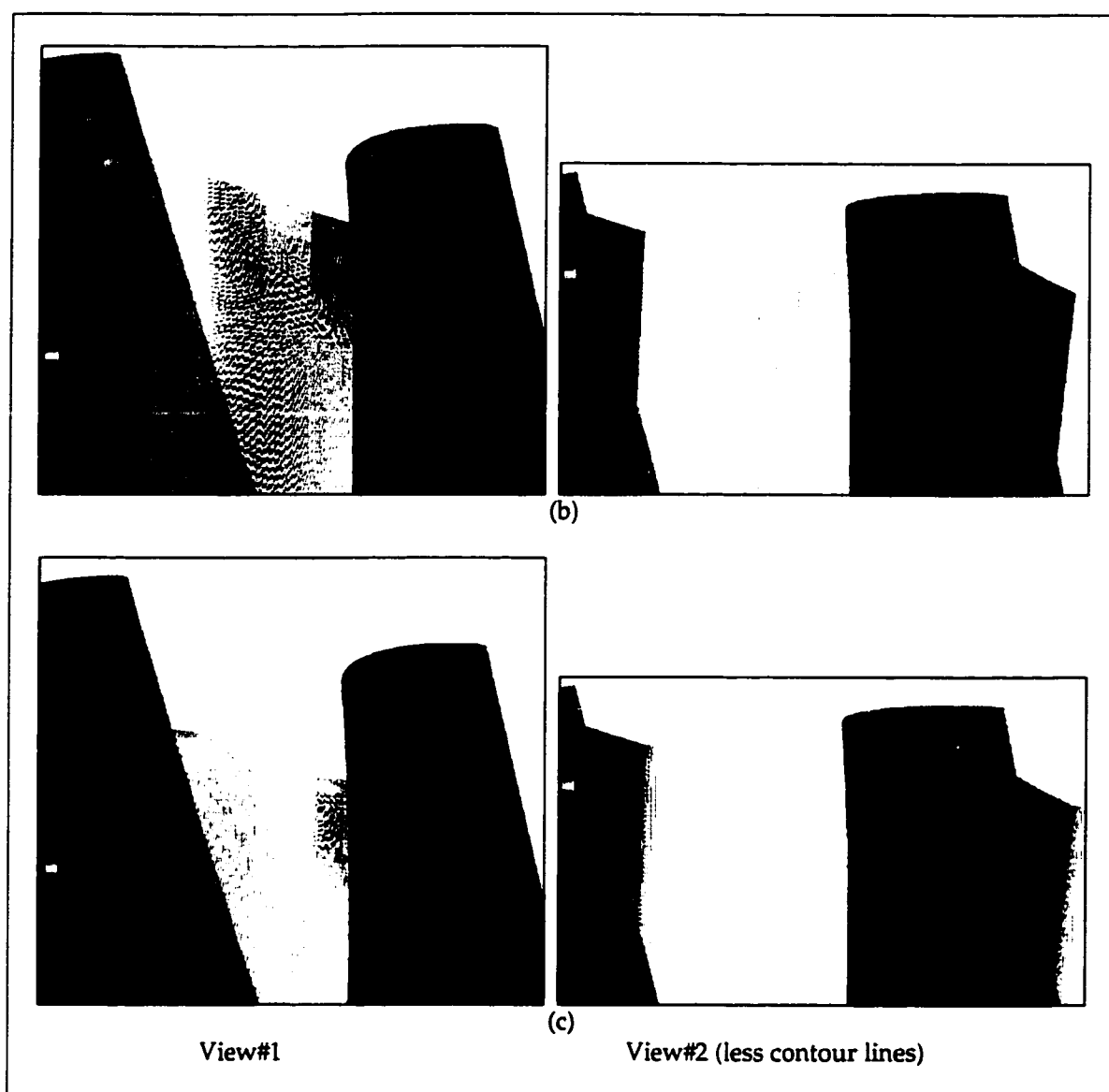


Figure 3.1.1-2 (suite) Static pressure contour lines: (a) at plane A (45.55% chord), (b) at plane B (50.70% chord), (c) at plane C (99.50% chord).

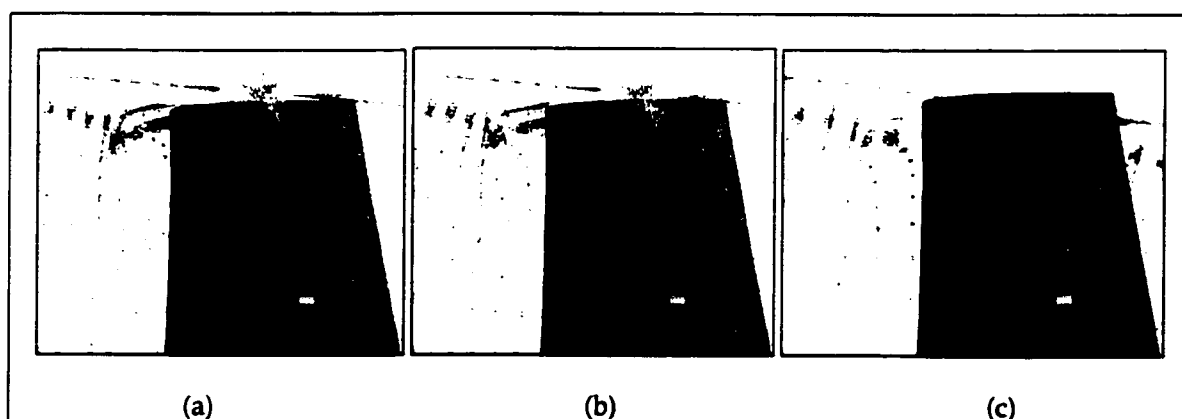


Figure 3.1.1-3 Velocity vectors: (a) at plane A, (b) at plane B, (c) at plane C. Note: the colours here represent the static pressure variations.

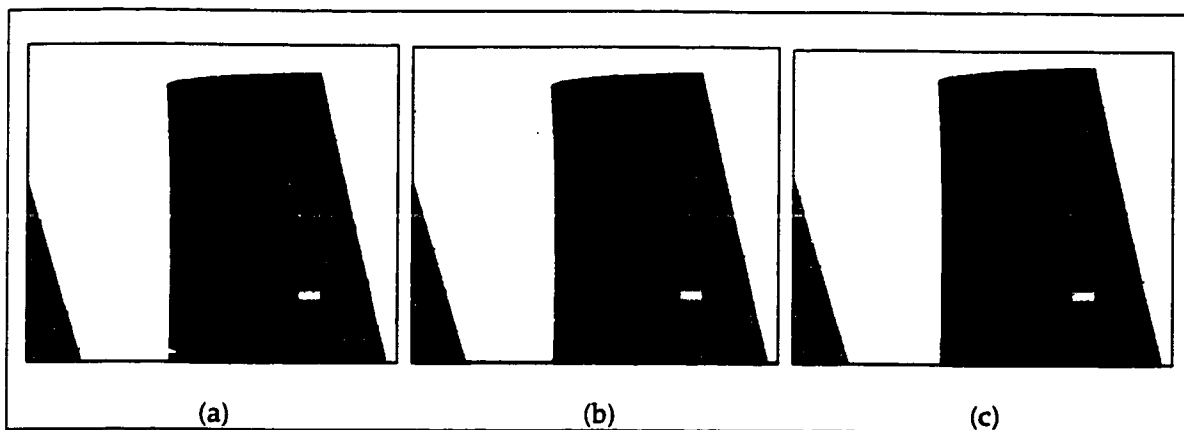


Figure 3.1.1-4 Mach number contour lines: (a) at plane A, (b) at plane B, (c) at plane C.

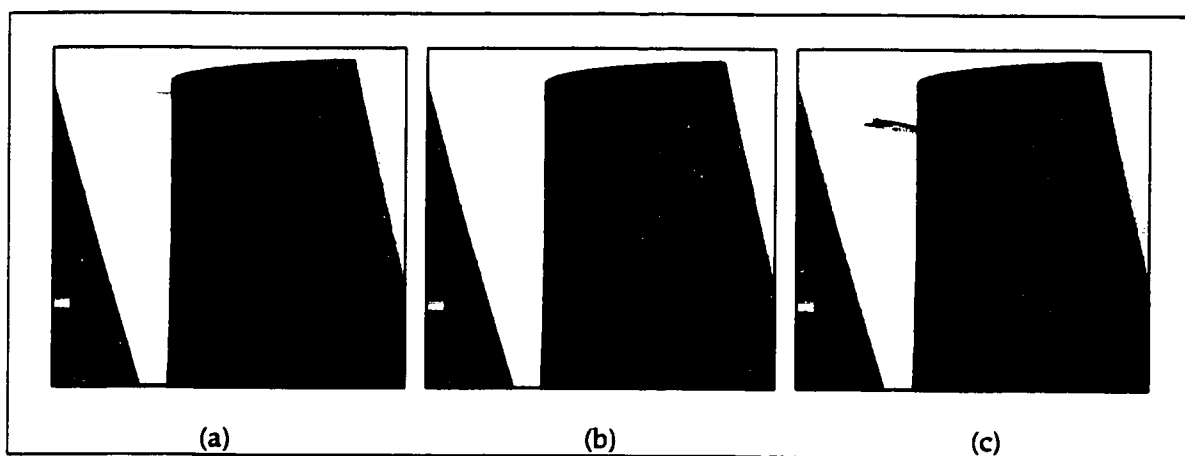


Figure 3.1.1-5 Entropy contour lines: (a) at plane A, (b) at plane B, (c) at plane C.

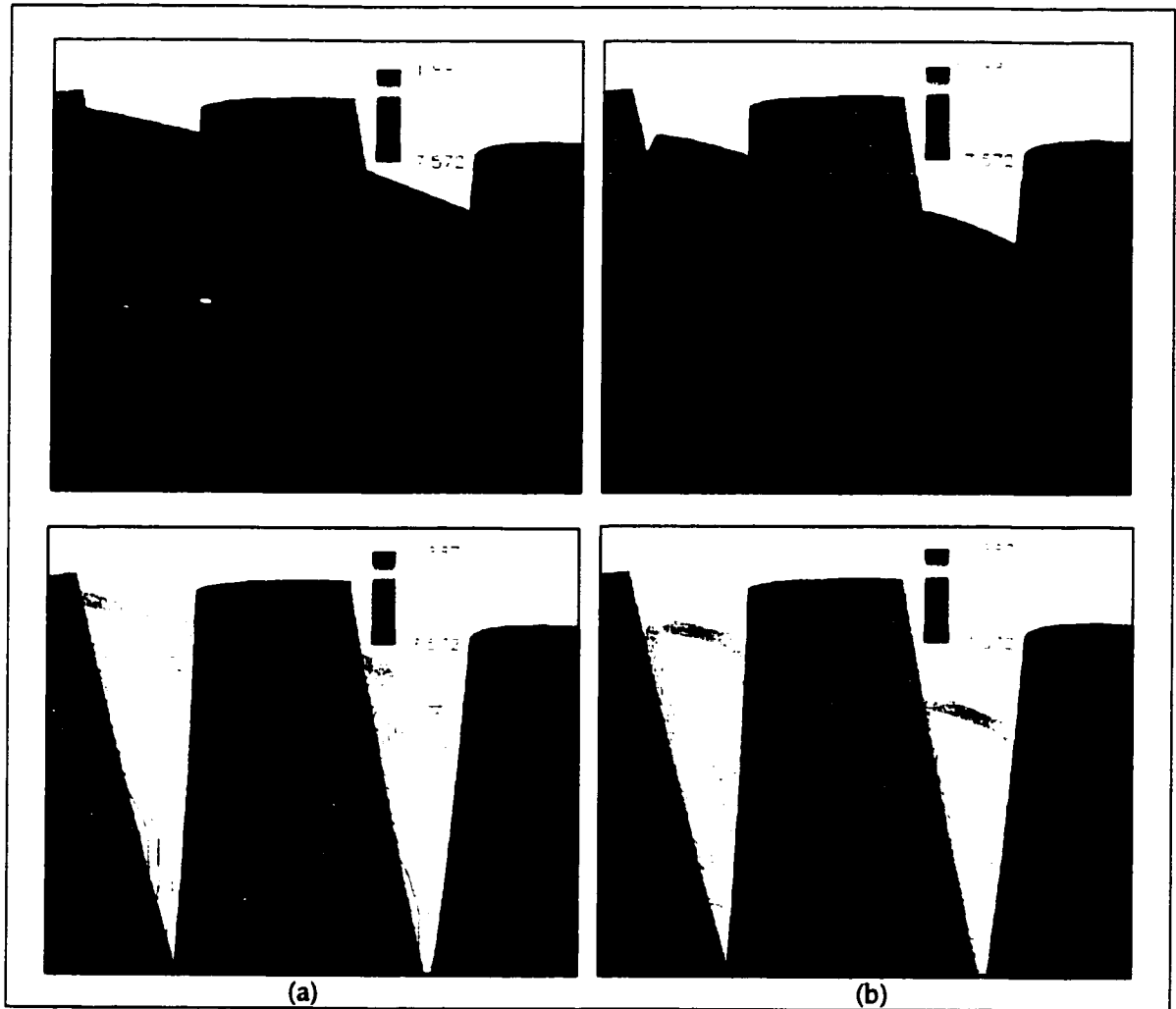
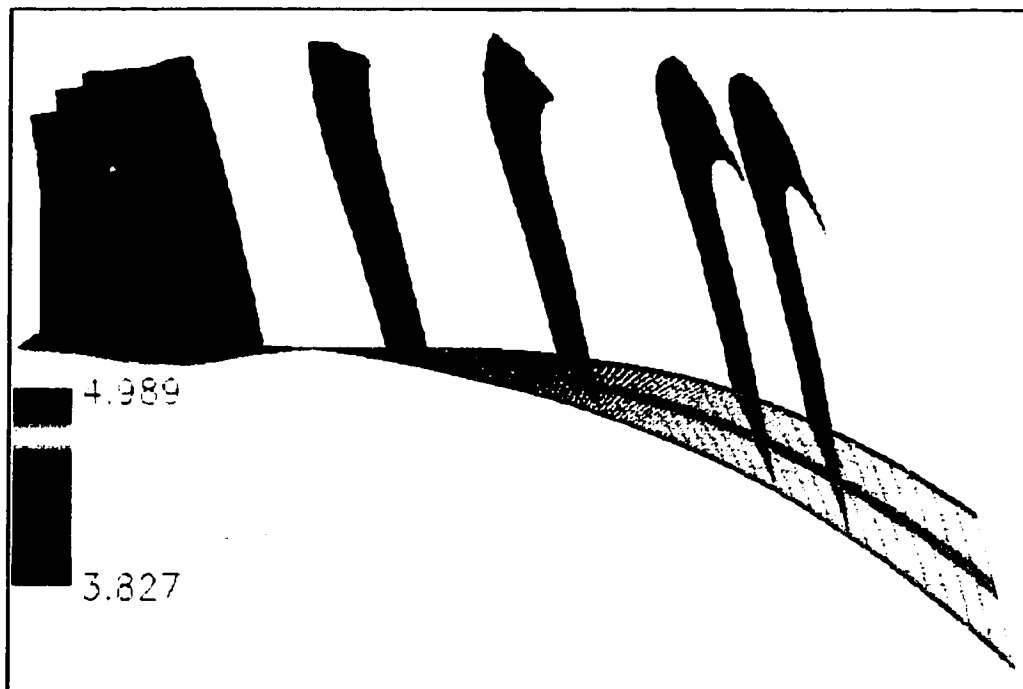


Figure 3.1.1-6 Vortices merge: Entropy distribution & contour lines:
 (a) two vortices at plane D (TE + 0.16 chord), (b) one vortex (merged vortices) at plane E (TE + 0.41 chord).



(a)



(b)

Figure 3.1.1-7 Evolution of the vortex: Entropy distribution at different planes F(TE), G(TE + 1 chord), H(TE + 2 chord), I(TE + 3 chord) and J(TE + 3.47 chord).

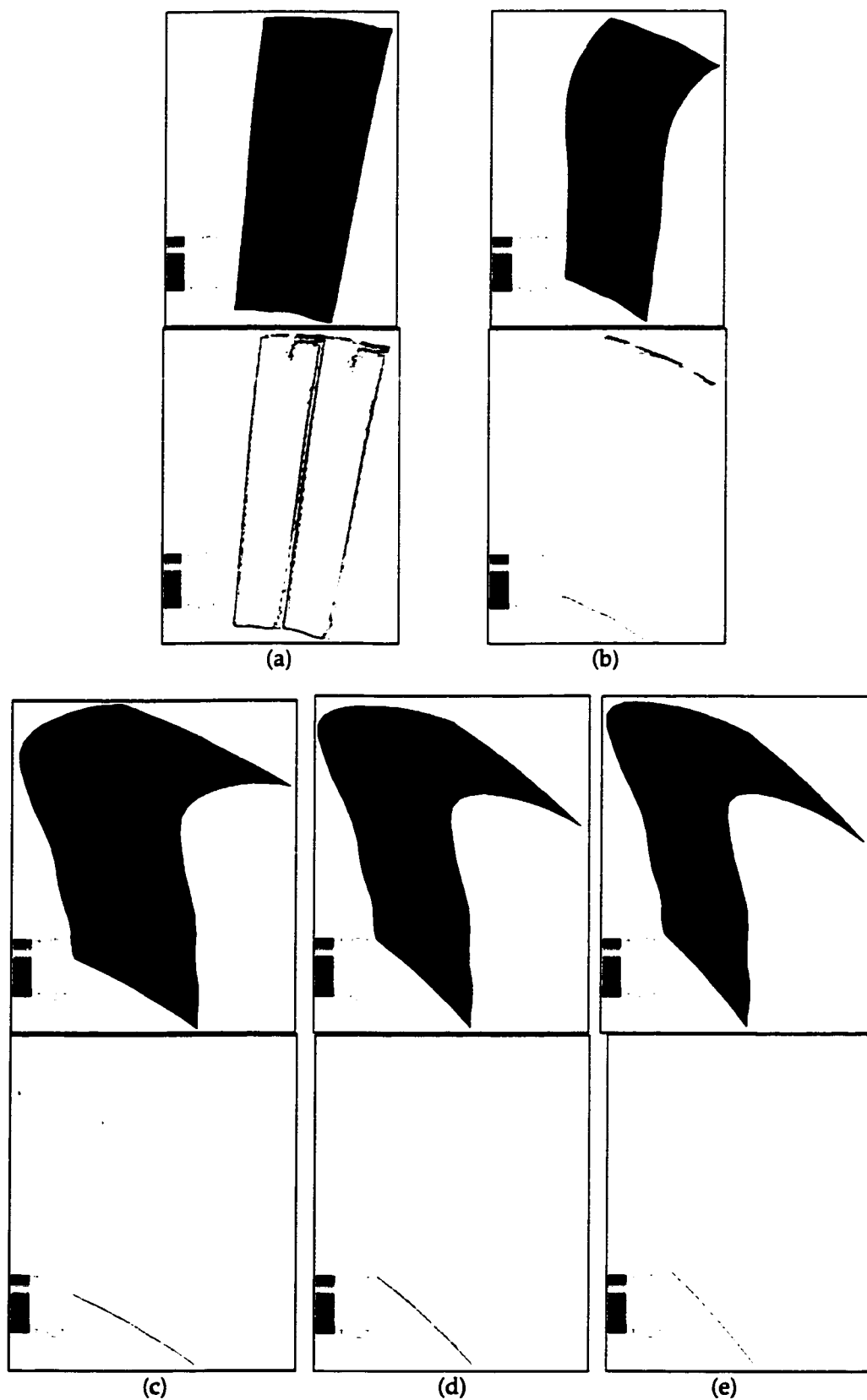


Figure 3.1.1-8 Entropy distribution and contour lines: (a) at plane F, (b) at plane G, (c) at plane H, (d) at plane I, (e) at plane J.

3.2. Effect of blade speed (RPM) on performance characteristics of high-pressure turbine stage

As mentioned earlier (chapter 1), an aircraft engine has a wide operating envelope (take-off, climb, cruise, descent and landing), and thus does not always run at its design speed. Also, engine deterioration and variation in atmospheric conditions are other important reasons causing the engine not to run at its design speed. This has an important impact on the engine (turbine) efficiency, and thus on the fuel consumption. All of that makes it necessary to understand the effect of variations of blade speed on the efficiency of the turbine.

In order to understand the effect of varying blade speeds, a simple 1-D analysis using velocity triangles is helpful. Figure 3.2-1 shows that for a typical gas turbine (and assuming constant C_x (axial velocity), α_1 and β_2), the decrease in speed will result in an increase of incidence on the blade. Whereas for an increase of blade speed, the incidence is expected to decrease.

The 3-D predictions of *NS3D* as well as, turbine correlations and experimental data are presented in Figure 3.2-2. This graph plots the change in efficiency, normalized with respect to the design point value, versus blade speeds at constant pressure ratio. The graph shows that for speeds below the design speed, all three curves agree on the fact that efficiency drops significantly.

Whereas for speeds above the design value, a continuous increase in efficiency is shown by the experimental and *NS3D* curves (Table 3.2-1). Turbine correlations show peak efficiency at 110% design speed, and then, a decrease in efficiency is noticed for the 120% design speed case. Comparison of these results with those presented by Vlasic et al. (1996) [56] and Woinowsky-Krieger et al. (1998) [60] shows similar trends.

These results demonstrate the impact of running at speeds below the design value. For example, being 5% short of design speed will result in around 1% decrease in stage efficiency (see figure 3.2-2), which can mean roughly more than 1% in specific fuel consumption for a typical turbofan engine [60]. The results of Figure 3.2-2 are qualitatively substantiated by *NS3D* predictions of losses (DELP/P) found in Table 3.2-2, in which it is shown that losses increase by decreasing speed.

From *NS3D* results, surface Mach number distribution plots for the vane and blade were obtained at mean radius for the different speeds, and they are shown in Figures 3.2-3 and 3.2-4. These plots show that the variation of blade speed, which had caused changes in the flow conditions on the blade, has resulted in some variations in the vane back pressure. These variations in the vane back pressure had affected the Mach number profile in the vane exit area. This is very well depicted in Figure 3.2-3.

From Table 3.2-2, It has been found that the vane exit Mach number varies from 1.24 at 70% $(N/\sqrt{T})_{des}$ down to 1.14 at 120% $(N/\sqrt{T})_{des}$. Furthermore, Figure 3.2-4 shows that the variations in blade speed had a severe impact on the blade loading. *NS3D* predicted significant incidence changes in the blade leading edge area, which were found to be for the 70% $(N/\sqrt{T})_{des}$, 10.6° increase in incidence from 100% $(N/\sqrt{T})_{des}$, and a drop of 13.7° for the 120% $(N/\sqrt{T})_{des}$ from 100% $(N/\sqrt{T})_{des}$. This variation of incidence had a pronounced effect on the Mach number in the inlet region. The inlet peak Mach number reaches a value as high as 1.88 (for the 70% $(N/\sqrt{T})_{des}$). Whereas for the 100% $(N/\sqrt{T})_{des}$ speed and higher, the inlet Mach number was completely subsonic. The drop in blade speed had also resulted in a significant increase of Mach number in the exit region. The peak exit Mach number is found to drop from 1.68 at 70% $(N/\sqrt{T})_{des}$ to around 1.4 at 120% $(N/\sqrt{T})_{des}$. This drop in Mach number gives a reasonable explanation of the increase of stage efficiency for the speed range studied.

Figure 3.2-5 shows predicted stage reaction (Table 3.2-3) versus speed. From this figure, it is noticed that the reaction is minimum near 80% $(N/\sqrt{T})_{des}$, thereafter, increasing on either side with a steeper rising slope on the low speed side. By

comparing the variation in reaction with the variation of blade incidence losses, certain similarity in their trend is found, much like the finding in reference [60].

Blade Speed (RPM) (section 3.2)

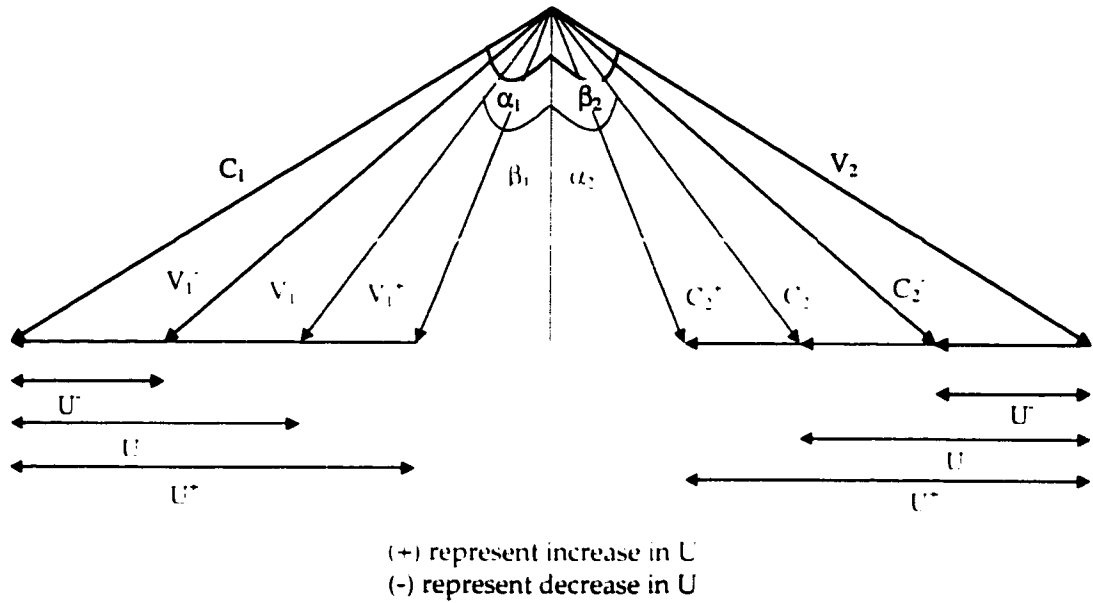


Figure 3.2-1 Effect of varying blade speed on the velocity triangle.

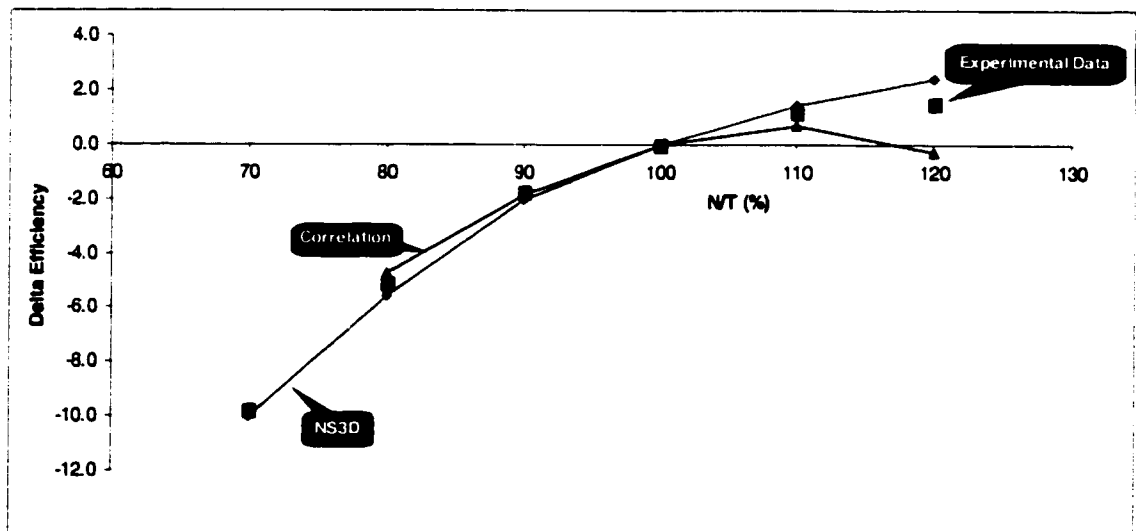


Figure 3.2-2 NS3D predictions for the variation of stage efficiency vs. blade speed.

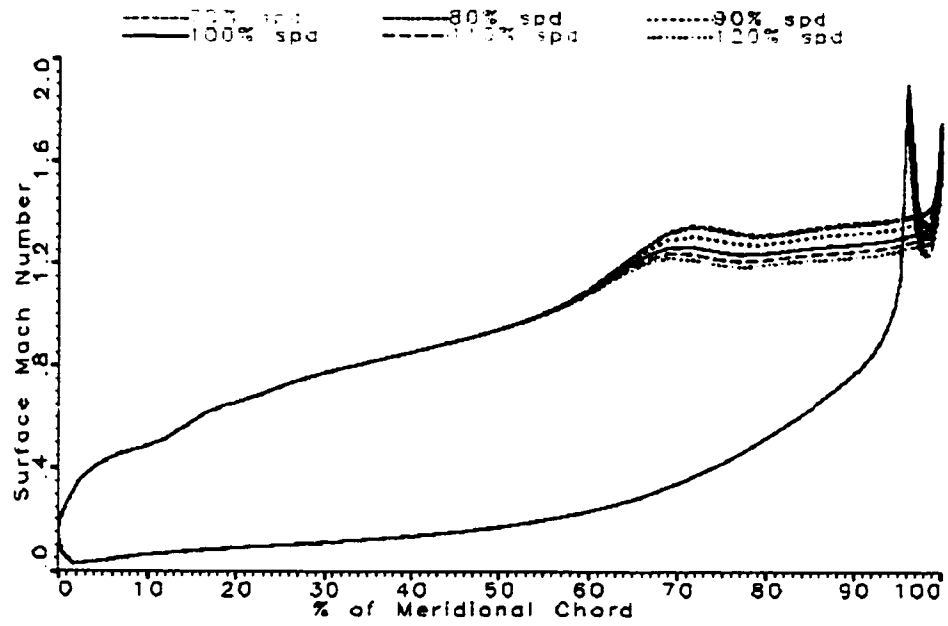


Figure 3.2-3 NS3D predictions for vane mid-span Mach number distribution, for all blade speeds.

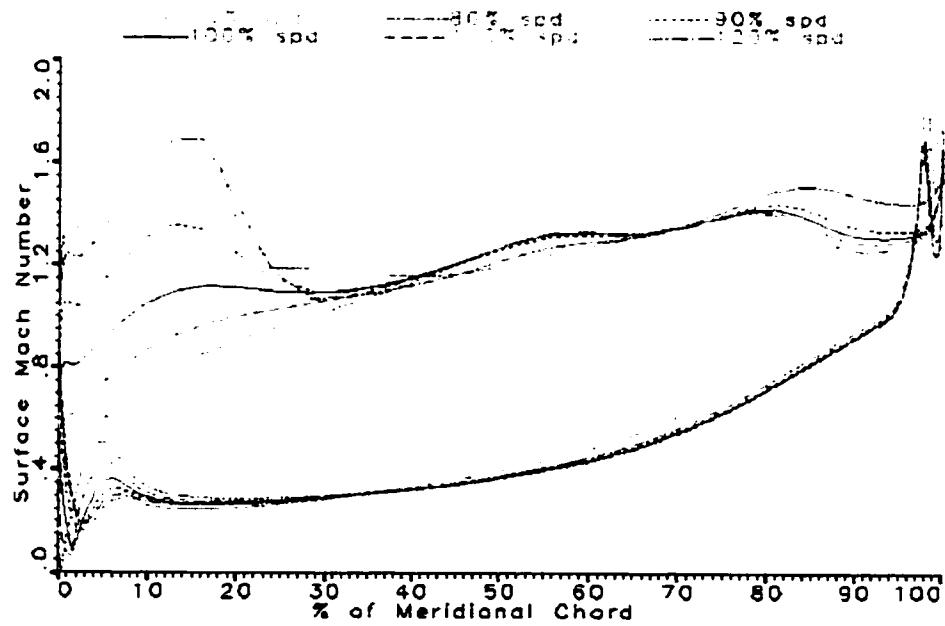


Figure 3.2-4 NS3D predictions for blade mid-span Mach number distribution, for all blade speeds.

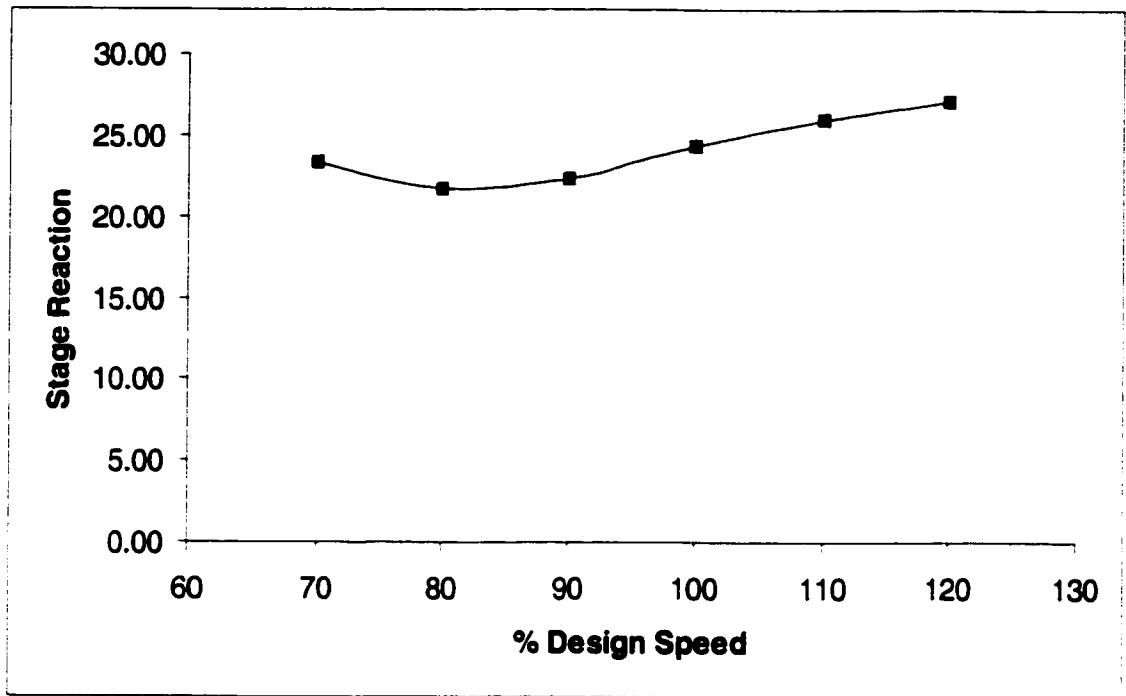


Figure 3.2-5 NS3D predictions for averaged stage reaction, for all blade speeds.

Blade Speed (RPM) (section 3.2)

	80 %spd	90 %spd
Pt1	13.9980	13.9980
Pt4	3.4377	3.4466
Tt1	770.0000	770.0000
Tt4	599.7600	592.5793
Tavg=(Tt1+Tt4)/2	689.8800	686.2897
Gamma(Tavg)	1.3971	1.3973
ETA(effic. %)	79.026	81.969
%ETA diff. from 100% code	-5.54	-2.04

Table 3.2-1 Stage efficiency of the six blade speeds.

	80 %spd	90 %spd
Vane: From -10% LE to GAP COMP AVERAGED DOWNSTREAM		
Pt1a	13.9772	13.9772
Pt2	12.6163	12.6469
DELP/P	0.0974	0.0962
M2	1.2370	1.2100
Blade: From -10% LE to +10% TE		
Swirl(r)2a	58.5981	55.1699
Delta Swirl2a from Design	6.0073	4.5781
Pt2a	6.8391	6.6105
Pt3	5.9418	5.8729
DELP/P	0.1312	0.1116
Mr3	1.1890	1.1370
M3	0.7750	0.6980
Swirl(r)3	65.9820	56.3750
Duct: From +10% TE to measuring plane		
Pt3	3.7735	3.6353
Pt4	3.5541	3.4466
DELP/P	0.0561	0.0519
Mr4	1.0760	1.0520
M4	0.579	0.509
Swirl(r)4	63.418	64.255
Swirl4	36.48	28.27

Table 3.2-2 Stage detailed analysis for the all blade speeds studied.

	80 %spd	90 %spd
P1	13.7810	13.7810
P2	4.9112	5.1272
P3	2.4692	2.6332
R(%)	21.765	22.3719
%R from R(des)	-10.5312	-8.0848

Table 3.2-3 Influence of blade speed on the stage reaction.

3.3. Effect of Pressure Ratio (PR) on performance characteristics of high-pressure turbine stage

As mentioned previously, since a gas turbine engine operates at different conditions, thus, the components of the engine such as the turbine will have a different operating condition (such as the stage pressure ratio) than the design one. Also, the use of an existing design for a new application by using an existing hardware with airfoil restagger and change in pressure ratio will sometimes suffice for a new engine derivative for a new application [60]. All of that makes the understanding of the effect of running the turbine at an off-design PR a very important step in the process of predicting the engine overall performance.

In a similar way to the analysis of the effect of variation of blade speed, a simple 1-D analysis using velocity triangle is helpful in understanding the effect of varying turbine stage pressure ratio. Figure 3.3-1 shows that for a typical gas turbine (and assuming constant U , α_1 and β_2), the decrease in PR will result in a decrease of the axial velocity which will result in a decrease of the incidence on the blade, whereas for an increase of PR the axial velocity will increase, and thus the incidence is expected to increase.

NS3D has been used to analyse the effect of variation of the turbine stage pressure ratio (Table 3.3-1). Figure 3.3-2 plots the change of efficiency normalized with respect to the design point value versus a range of PR at a constant blade speed (the design speed). Despite the fact that the range of PR studied is very large, the prediction of *NS3D* gives reasonable results for PR higher than the 90% PR_{des} . For PR lower than this value, however, the code is less sensitive to the variation of PR than are the experimental data. The figure also shows that *NS3D* predictions compare more favorably to the test results than those obtained by the turbine correlation predictions. This figure reveals the fact that for any increase or decrease of the stage pressure ratio from the design value (100% PR_{des}), the efficiency will drop, with this drop in the stage efficiency being more important for high-pressure ratios.

Figure 3.3-3 and 3.3-4 present the predicted *NS3D* vane and blade Mach number distributions for various PR at the design speed. Figure 3.3-3 shows that the vane is choked. Therefore, the vane exit swirl is practically constant and the exit Mach number is varying a little, as can be seen in Table 3.3-2. The vane exit Mach number is found to vary from 1.12 at 64.5% PR_{des} up to 1.17 at 76.3% PR_{des} , whereas, it is practically constant at 1.18 for 94% PR_{des} and higher.

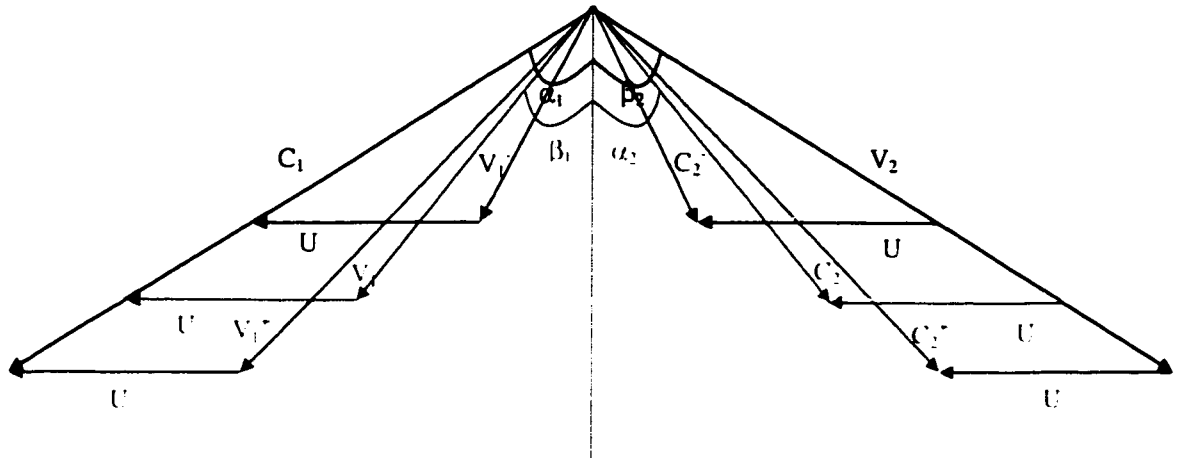
Thus, since the vane is choked, the inlet conditions to the blade remain almost unchanged (particularly for the 94% PR_{des} and higher cases), and as seen in figure 3.3-4, all the additional loading resulting from the increase in PR is taking place entirely on the uncovered suction surface.

Figure 3.3-5 plots the variation of the blade inlet and exit relative swirl. It indicates clearly that the variation in incidence on the blade is very small. It also shows that the blade exit relative swirl drops from its peak at 94% PR_{des} for any change in PR, but it is more significant for PR higher than 94% PR_{des} . This is very well translated into the big variation of the blade exit Mach number as seen in Table 3.3-2 and figure 3.3-4. The peak Mach number, in the blade exit area is found to vary from 1.1 at 64.5% PR_{des} to around 1.7 at 113% PR_{des} . For the case of 121% PR_{des} , the very high value of the peak exit Mach number found (around 2.6 from figure 3.3-4) is believed to be too high and thus non-physical. It is most probably due to the mesh skewness in that region, so as PR increases, the overshoot in Mach number becomes more significant, and thus, non-physical.

The prediction of the stage mean reaction is shown in figure 3.3-6 and Table 3.3-3. The reaction increases from 11% for 64.5% PR_{des} to around 28% for 121.3% PR_{des} . This figure shows that PR has a significant effect on reaction, and it is

more important than that of the speed (as seen in the previous section). This is due to the fact that at very low PR's, the vane takes up most of the available static pressure drop. For higher PR's, however the vane becomes choked, and, therefore, the blade increases its static pressure drop, which yields an increase of the reaction.

Pressure Ratio (section 3.3)



(+) represent increase in PR
(-) represent decrease in PR

Figure 3.3-1 Effect of varying pressure ratio on the velocity triangle.

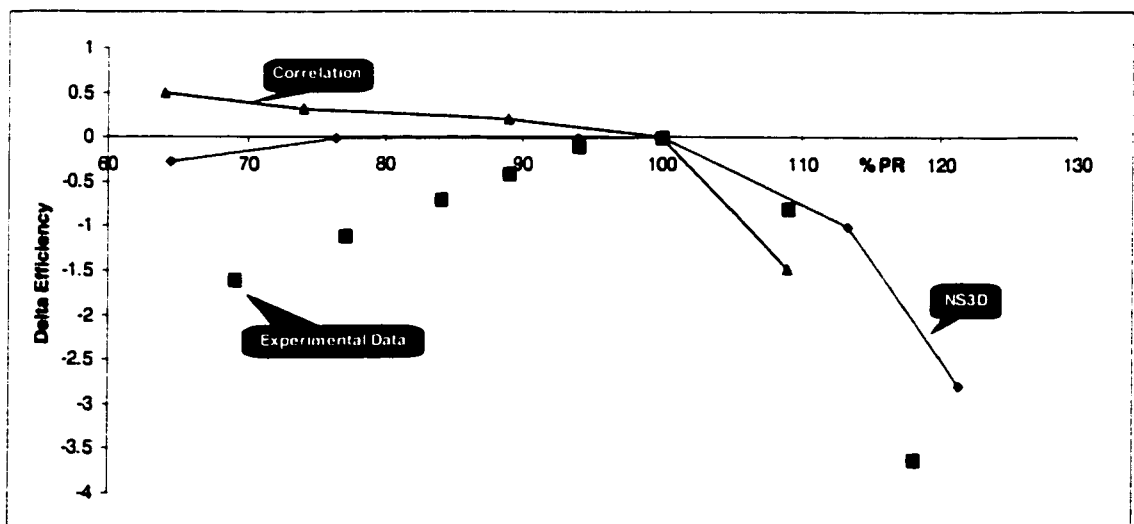


Figure 3.3-2 NS3D predictions for the variation of stage efficiency vs. stage pressure ratio.

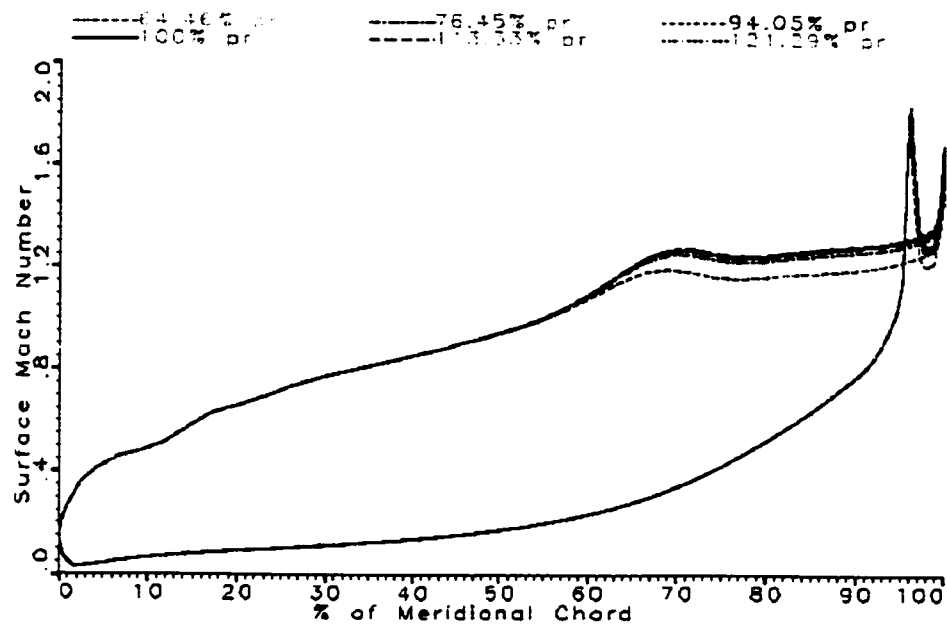


Figure 3.3-3 NS3D predictions for vane mid-span Mach number distribution, for the six PR's studied.

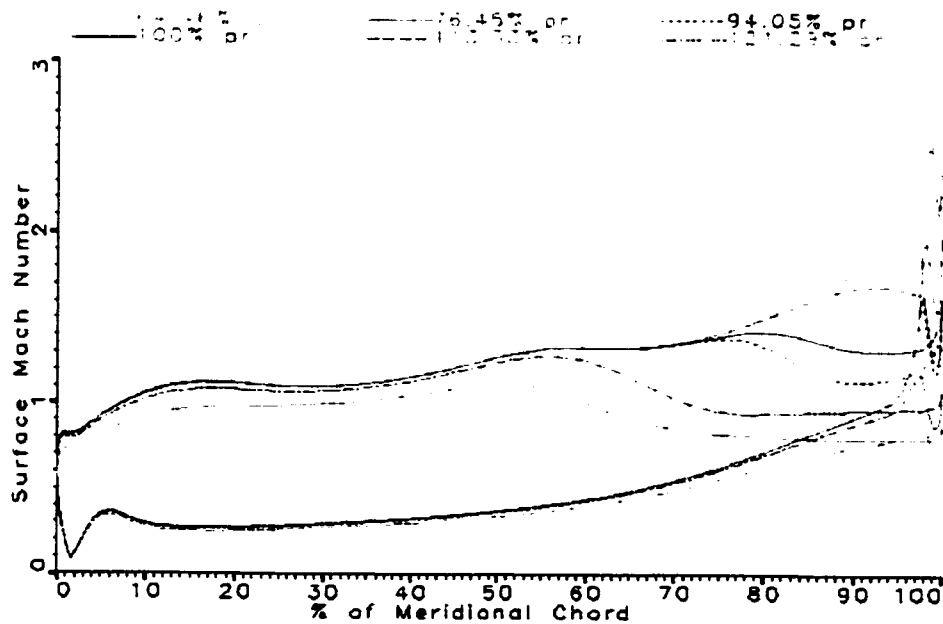


Figure 3.3-4 NS3D predictions for blade mid-span Mach number distribution, for the six PR's studied.

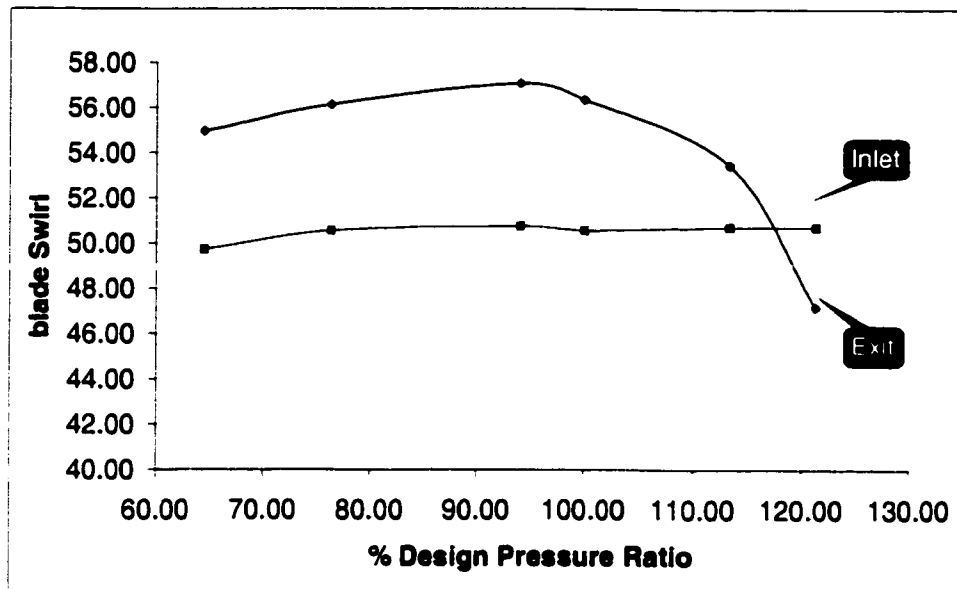


Figure 3.3-5 NS3D predictions for blade in and out relative swirl, for the range of stage pressure ratio studied.

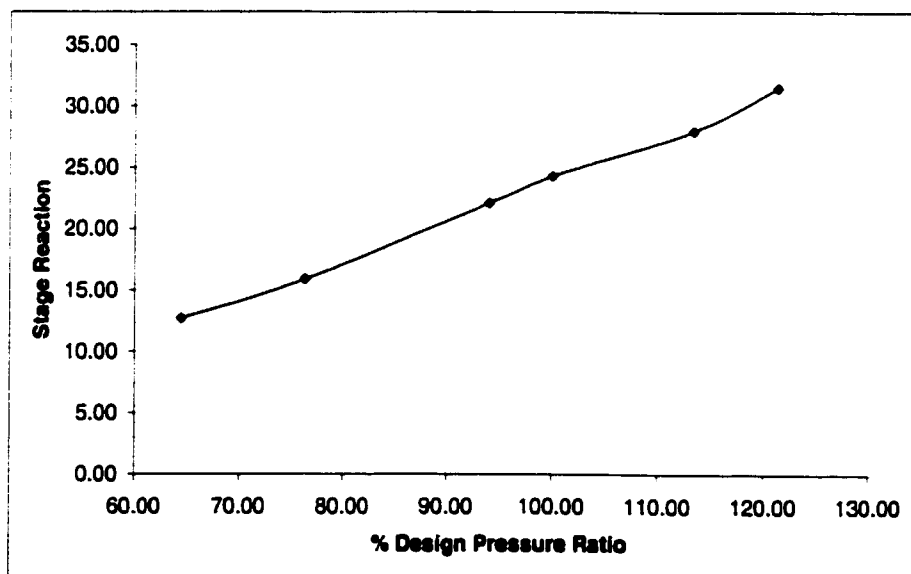


Figure 3.3-6 NS3D predictions for average stage reaction, for the range of stage pressure ratio studied.

Pressure Ratio (section 3.3)

	76.34 % PR	94.04 % PR
Pt1	13.9880	13.9880
Pt4	4.4313	3.5972
Tt1	770.0000	770.0000
Tt4	590.5083	563.6436
Ttavg=(Tt1+Tt4)/2	680.2532	666.8218
Gamma(Ttavg)	1.3966	1.3973
ETA(effic. %)	83.630	83.628
% ETA diff. from 100% code	-0.01	-0.01

Table 3.3-1 Stage efficiency for the six stage pressure ratios.

	76.34 % PR	94.04 % PR
Vane: From -10% LE to GAP COMP AVERAGED DOWNSTREAM		
Pt1a	13.9773	13.9772
Pt2	12.734	12.7013
DEL P/P	0.0890	0.0913
M2	1.1680	1.1840
Blade: From -10% LE to +10% TE		
Swirl(r)2a	50.5637	50.7736
Delta Swirl2a from Design	-0.0051	0.1847
Pt2a	6.5905	6.4884
Pt3	6.0638	5.8538
DEL P/P	0.0769	0.0978
Mr3	0.8260	1.0470
M3	0.4820	0.5990
Swirl(r)3	56.1710	57.0860
Inter-Turbine-Duct: From +10% TE to measuring plane		
Pt3	4.5639	3.7357
Pt4	4.4313	3.5972
DEL P/P	0.0291	0.0371
Mr4	0.8090	0.9940
M4	0.346	0.435
Swirl(r)4	65.082	64.799
Swirl4	10.02	13.90

Table 3.3-2 Stage detailed analysis for the range of pressure ratios studied.

	76.34 % PR	94.04 % PR
P1	13.7810	13.7810
P2	5.4665	5.3359
P3	3.8860	2.9334
R (%)	15.9257	22.1474
% R from R(des)	-34.5692	-9.0089

Table 3.3-3 Influence of stage pressure ratio on the turbine stage reaction.

3.4. Effect of Vane Stagger Angle on performance characteristics of high-pressure turbine stage

The stagger angle is the angle between the airfoil axial chord and the airfoil chord (see figure 1-5 in chapter 1 for blade terminology). In this chapter, the term “closing” the vane is used to indicate that the vane stagger angle is increased, and therefore closing the throat (reducing the throat area), from which the term “closing” comes.

Experience has shown that manufacturing in general introduces some imperfections in the stacking of the airfoils of the vane (and in the blade) and thus the stagger angle. So, some testing and adjustment to the stagger angle has to be done before sending the component to a full production. The design parameter used as a criteria to determine if the obtained vane is matching the requirement of the design, is known as the ‘Flow Capacity’ (Q), which is represented by $m\sqrt{T_{t1}}/P_{t1}$.

Thus, the stagger angle of the vane has an important impact on the performance of the turbine stage, since it influences the inlet Mach number to the blade and certainly the incidence. As will be discussed later, the losses in a turbine stage will vary (increase or decrease) for even a minimal change in the vane stagger angle.

In order to study the effect of the change of the vane stagger angle, four tests have been conducted. The first two are without closing the vane and at two different blade speeds ($70\% (N/\sqrt{T})_{des}$ & $100\% (N/\sqrt{T})_{des}$) and the other two were with a closed vane for the same blade speeds of the first two cases. Thus, the effect of the speed could also be studied.

With the vane stagger angle closed by only 0.8° , interesting results are found. *NS3D* predictions of the stage isentropic efficiency for the four test cases are plotted in figure 3.4-1 (Due to the lack of experimental data from the CFTR used, only the results of *NS3D* are presented). The code predicts that (see Table 3.4-1) by closing the vane by only 0.8° , a slight increase in stage efficiency was noticed for the $70\% (N/\sqrt{T})_{des}$, whereas, a significant drop in efficiency was detected for the $100\% (N/\sqrt{T})_{des}$.

Figure 3.4-2 shows that closing the vane results in a higher vane exit Mach number for the two different blade speeds. For the $70\% (N/\sqrt{T})_{des}$, the vane exit Mach number (see Table 3.4-2) has increased from 1.21 to 1.24 whereas it has increased from 1.15 to 1.18 for the $100\% (N/\sqrt{T})_{des}$, as it could be seen in Table 3.4-2. The change of the blade incidence resulting from closing the vane is: an

increase of around 1.1° for the 70% $(N/\sqrt{T})_{des}$ and an increase of 2.2° for the 100% $(N/\sqrt{T})_{des}$. As a consequence, the flow entering the blade has been affected, and an increase in Mach number is noticed in figure 3.4-3. A much bigger change is detected in the blade exit Mach number, however, especially for the 70% $(N/\sqrt{T})_{des}$. The peak Mach number in the blade exit area has increased from 1.55 to 1.68 for the 70% $(N/\sqrt{T})_{des}$, and has decreased from 1.5 to 1.42 for the 100% $(N/\sqrt{T})_{des}$. Thus, for this studied turbine, it was found that at low blade speeds (such as the 70% $(N/\sqrt{T})_{des}$), a small closing in the vane stagger angle results in a steep increase of exit Mach number. Whereas for high blade speeds (such as the 100% $(N/\sqrt{T})_{des}$), the same change in the vane stagger angle results in a small decrease of exit Mach number.

The stage reaction predictions are plotted in figure 3.4-4 (see also Table 3.3-3). It is clear from the figure that closing the vane stagger angle by 0.8° resulted in a decrease in reaction for the two-tested blade speeds. A slightly higher decrease in reaction is found for the 70% $(N/\sqrt{T})_{des}$. This leads to the conclusion that closing the vane by such small value has the same relatively negative effect (causing a drop) on the stage reaction, independent of the blade speed.

Vane stagger angle (section 3.4)

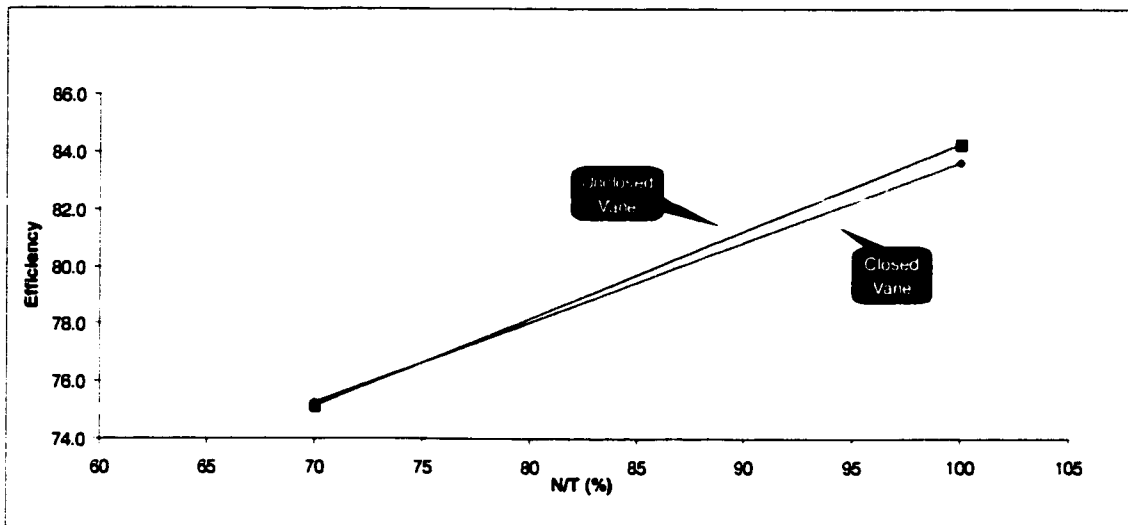


Figure 3.4-1 NS3D predictions of stage efficiency for the effect of closing vane stagger angle by 0.8° .

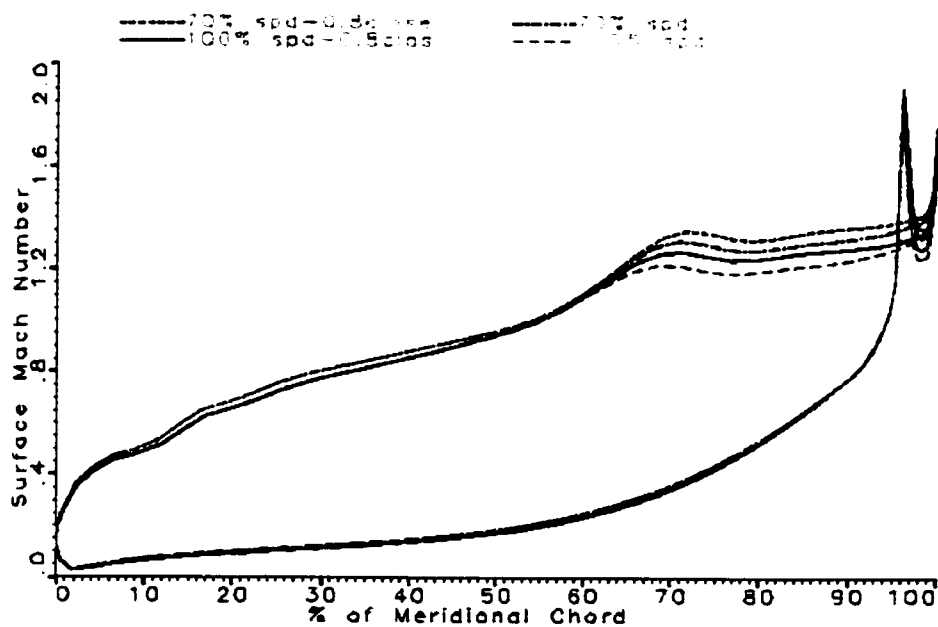


Figure 3.4-2 NS3D predictions for vane mid-span Mach number distribution for the two speeds and vane stagger angles.

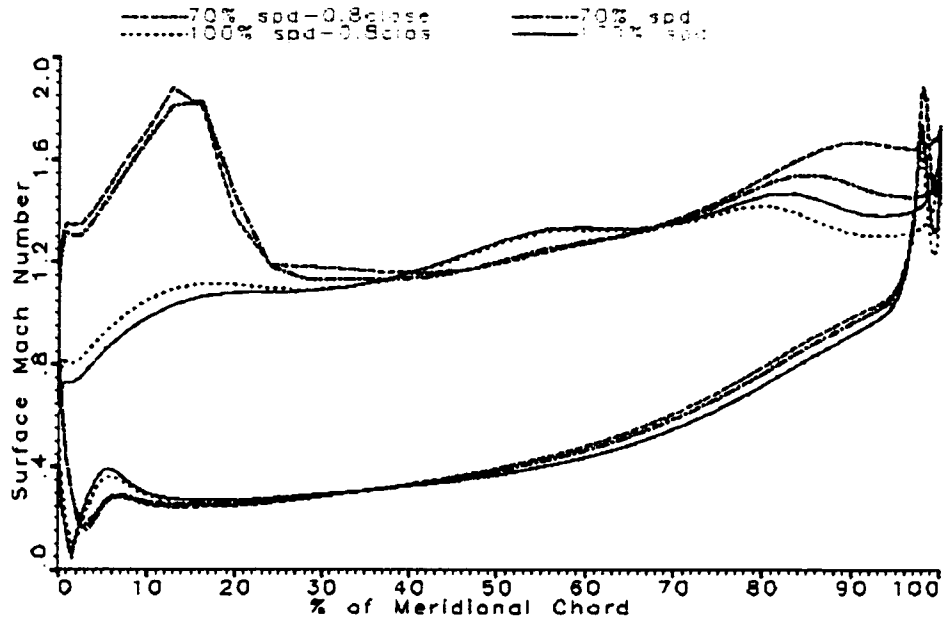


Figure 3.4-3 NS3D predictions for blade mid-span Mach number distribution for the two speeds and vane stagger angles.

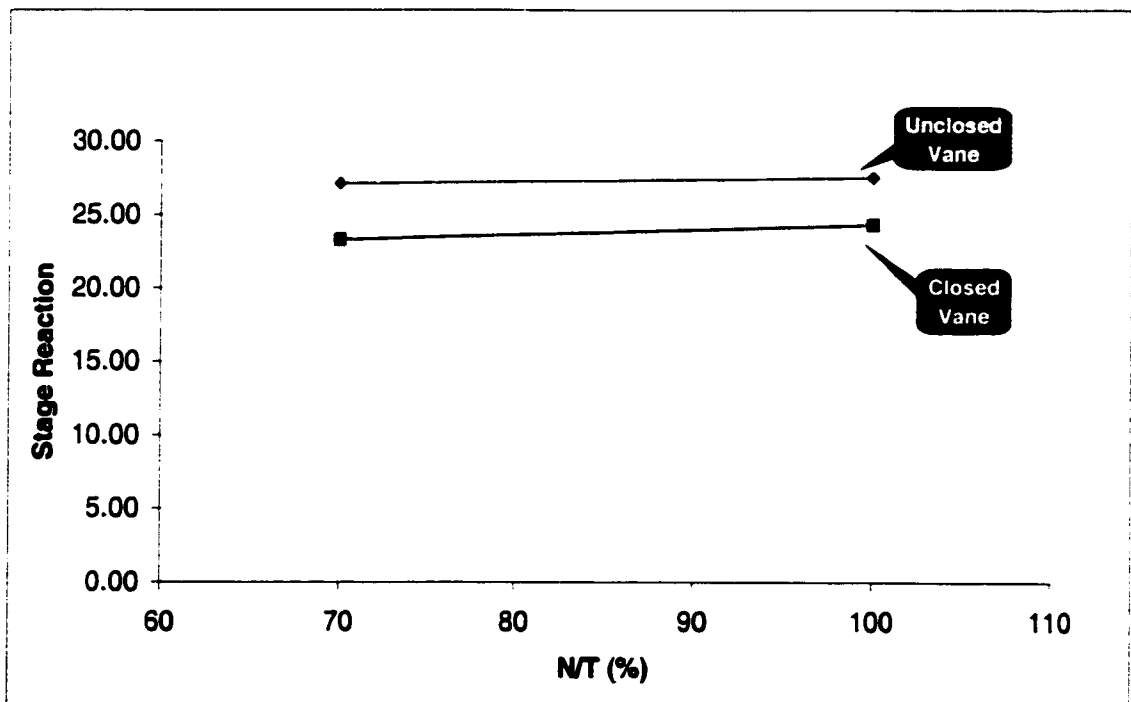


Figure 3.4-4 NS3D predictions for averaged stage reaction for the two speeds and vane stagger angles.

Vane Stagger Angle (section 3.4)

	Closed Vane	Unclosed Vane	% difference of closed from unclosed vane
Pt1			
Pt4			
Tt1			
Tt4			
$T_{avg} = (Tt1 + Tt4)/2$			
$\Gamma(T_{avg})$			
ETA(effic. %)			
% ETA diff. from 100% code			

Table 3.4-1 Stage efficiency and comparison for the closed and unclosed vane at the two speeds.

	Closed Vane	Unclosed Vane	% difference of closed from unclosed vane
Vane: From -10% LE to GAP COMP AVERAGED DOWNSTREAM			
Pt1a			
Pt2			
DEL P/P			
M2			
Blade: From -10% LE to +10% TE			
Swirl(r)2a			
Del. Swirl2a from Des. Spd			
Ptr2a			
Ptr3			
DEL P/P			
Mr3			
M3			
Swirl(r)3			
Duct: From +10% TE to measuring plane			
Pt3			
Pt4			
DEL P/P			
Mr4			
M4			
Swirl(r)4			
Swirl4			

Table 3.4-2 Stage detailed analysis and comparison for the closed and unclosed vane at the two speeds.

	Closed Vane	Unclosed Vane	% difference of closed from unclosed vane
P1			
P2			
P3			
R (%)			
% R from R(des)			

Table 3.4-3 Influence of vane stagger angle and blade speed on the stage reaction.

4. Discussions

4.1 Accomplishments and Conclusion

Using a 3-D viscous, compressible code (*NS3D*) that solves the three-dimensional, Reynolds averaged Navier-Stokes equations, CFD-based correlations have been produced for a single stage high-pressure transonic turbine. Four design and off-design parameters were studied, and their effects on the performance characteristics of the turbine were discussed. Each of the above mentioned parameters was studied in detail and relevant phenomena, such as the tip leakage vortex, were analyzed. All of the results obtained from *NS3D* were compared to an existing turbine correlation and to experimental data, except the tip clearance and vane stagger angle cases for which no test data are available from the CFTR test case used.

In general, the code compared favourably to the experimental values except for the PR cases, where the code was found to be insensitive to the variations of pressure ratios lower than 90% PR_{des} . This is due to the relatively coarse mesh used, since the code is still under development and since these runs were the first runs obtained from the code for turbines. It can also be explained by the

implementation of the boundary (see next section) conditions (constant profile imposed at inlet and imposed static pressure at the hub of the exit plane). Nevertheless, the results obtained from the code are still considered satisfactory. No tests were conducted on the effect of denser mesh on the solution, since much longer running time will be required, but experience has shown that a denser mesh (to a certain limit) will improve the results in general.

From the first parameter studied, it has been found that increases in the tip clearance have significant negative impact on the turbine stage efficiency. The blade loading distribution from hub to tip has been found to vary by varying the tip clearance, as found by Amrud and Sjolander (1986) [3], whereas the vane seems to be unaffected by this phenomenon. The stage reaction also did not vary by much for the various tip clearances.

The code was able to give a good understanding and interesting simulation of the tip leakage vortex. It was found to get bigger and stronger as the tip clearance increases. It has also been found that multiple vortices could be generated for relatively big tip clearances, which confirms again the findings of reference 3.

The blade speed effect was the best example of the agreement of *NS3D* results with the experimental data. The highest offset was found to be less than 1% (of

the 100% case) at 120% design speed. In this analysis, it was shown that the turbine efficiency increases as the blade speed increases. Significant changes in the blade inlet Mach number have been found due to the change of vane exit Mach number. The reaction has been found to be minimal at around 80% $(N/\sqrt{T})_{des}$, and it increases for higher and lower blade speeds.

The analysis of the third parameter showed that any increase or decrease in the stage pressure ratio would result in a decrease in the stage efficiency. This is more important for the increase of PR. Also, it has been found that the code is not as sensitive to the decrease of PR as the experimental data is demonstrating. As expected, analysis of *NS3D* results showed that the vane is choked for all of the analysed PR's. It has been found, however, that the blade exit Mach number significantly increased as PR increases; which causes an important drop in blade exit swirl. This gives a very good explanation of the continuous increase of stage reaction predicted by *NS3D*, for the increase of PR.

The analysis of the vane stagger angle has demonstrated that increasing the vane stagger angle by very small quantity such as 0.8° has relatively the same important negative impact on the turbine stage efficiency, independent of the blade speed.

4.2 Future Work and Suggestions

Further investigation of different design and off-design parameters would give an even better understanding of the ability of *NS3D* to detect the effect of varying design and off-design parameters. The existence of some discrepancies between the experimental data and *NS3D* results suggests that a denser mesh could be helpful. This would await the possibility of dedicated time on more powerful computers and the full implementation of the CFD lab's Mesh Optimization methodology, MOM3D.

Due to the fact that in an internal flow environment the computation has to be performed on truncated domains, whose far-field boundaries do not represent an undisturbed known flow field as in external aerodynamics, imposing the static pressure at the outflow boundary will result in a reflective boundary condition. Since an outgoing unsteady pressure wave will produce an incoming pressure wave to keep the exit pressure constant. Similarly, unsteady reflections are generated at the inflow boundary through the specification of particular physical quantities [44]. So, implementing non-reflecting boundary conditions in the code would help to get more physical results, since this will improve transferring information across the stator/rotor interface in a manner that conserves fluxes of mass, momentum and energy, and avoids spurious reflections [24].

Since the flow in a turbomachine is unsteady, the results are expected to be more satisfactory if a full unsteady analysis is performed. This is in the works and is the subject of a Ph.D. thesis entitled *Simulation of 3-D Viscous Compressible Flow in Multistage Turbomachinery by Finite Element Methods* by Mohamad Sleiman (see reference [50]).

In order to gain more confidence in *NS3D*, a similar kind of analysis has to be performed on other types of turbines, and with multi-stage turbines. Only after that, one can use the code to create new design concepts and thus new reliable correlations.

References

1. Ainley, D.G, *The Performance Of Axial Flow Turbines*, Proceedings of the Institute of Mechanical Engineers, 1948, 159, p. 230.
2. Ainley, D.G, Mathieson, G.C.R., *An Examination Of The Flow And Pressure Losses In Blade Rows Of Axial Flow Turbines*, R. & M. No. 2891, A. R. C. Technical Report, Mar. 1951.
3. Amrud, K.K, Sjolander, S.A, 1986, *Effects Of Tip Clearance On Blade Loading In A Planar Cascade Of Turbine Blades*, ASME Paper 86-GT-245.
4. Bathie, W.W., *Fundamentals Of Gas Turbines*, John Wiley & Sons, New York, 1984, pp. 170, 237-238.
5. Benner, M.W, Sjolander, S.A, Moustapha, S.H, *Influence Of Leading-Edge Geometry On Profile Losses In Turbines At Off-Design Incidence: Experimental Results And An Improved Correlation*, ASME Journal of Turbomachinery, January 1997.

6. Binsley, R.L., Baljé, O.E, 1968, *Axial Turbine Performance Evaluation - Part A - Loss Geometry Relationships*, ASME Paper 68-GT-13.
7. Bogioian, J., Ni, R., 1989, *Prediction Of 3-D Multi-Stage Turbine Flow Field Using A Multiple-Grid Euler Solver*, AIAA Paper 89-0203.
8. Boretti, A., Martelli, F., 1986, *Development Of An Experimental Correlation For Transonic Turbine Flow*, ASME-86 Paper GT-108.
9. Boyce, M.P., *Gas Turbine Engineering Handbook*, gulf publishing, Houston, 1982, pp.1-35, 230-260.
10. Bryce, J.D, 1985, *Design Performance and Analysis Of High Work Capacity Transonic Turbine*, ASME Paper 85-GT-15.
11. Came, P.M., *Secondary Loss Measurements In A Cascade Of Turbine Blades*, Institute of Mechanical Engineers Conference Publication 3, 1973, pp. 75-83.
12. Came, P.M., Dunham, J, 1970, *Improvements To Ainley-Mathieson Method Of Turbine Performance Prediction*, ASME Paper 70-GT-2.

13. Camus, J.J., 1983, *Experimental And Computational Study Of Transonic Three Dimensional Flow In Turbine Cascade*, ASME Paper 83-GT-12.
14. Cohen, H., Rogers, G.F.C., Sarsvanamuttoo, H.I.H., *Gas Turbine Theory*, 4th ed., Addison Wesley Longman Limited, London, 1996, pp. 1-36, 271-320, 336-385.
15. Cox, H.J.A., Craig, H.R.M., *Performance Estimation Of Axial Flow Turbines*, Proceedings of the Institute of Mechanical Engineers, 1971, Vol. 185, No. 32, pp. 407-424.
16. Crow, D.E, Vanco, M.R, Welna, H, 1980, *Results From Tests On A High Work Transonic Turbine For An Energy Efficient Engine*, ASME Paper 80-GT-146.
17. Currie, T.C., Carscallen, W.E., 1996, *Simulation Of Trailing Edge Vortex Shedding In A Transonic Turbine Cascade*, ASME Paper 96-GT-483.
18. Davis, R.L, Shang, T, Buteau, J, Ni, R.H, 1996, *Prediction Of 3-D Unsteady Flow In Multi-Stage Turbomachinery Using An Implicit Dual Time-Step Approach*, AIAA Paper 96-2565.

19. Dawes, W.N, Leboeuf, F., Perrin, G., 1992, *Analysis of three-dimensional viscous flow in a supersonic axial flow compressor rotor with emphasis on tip leakage flow*, ASME Paper 92-GT-388.
20. Denton, J.D, *A Survey And Comparison Of Methods For Predicting The Profile Loss Of Turbine Blade*, Institute of Mechanical Engineers Conference Publication 3, Paper C76/73, 1973, pp. 204-212.
21. Dickens, T.E., Oldfield, M.L.G., Baines, N.C., Mee, D.J., 1990, *An Examination Of The Contributions To Loss On A Transonic Turbine Blade In Cascade*, ASME Paper 90-GT-264.
22. Dunham, J., *A Review Of Cascade Data On Secondary Losses In Turbines*, Journal Mechanical Engineering Science, Vol. 12 No.1, 1970, pp. 48-59.
23. Ewen, J.S., 1973, *Investigation Of The Aerodynamic Performance Of Small Axial Turbines*, ASME Paper 73-GT-3.
24. Giles, M.B., 1991, *UNSFLO: A Numerical Method For The Calculation Of Unsteady Flow In Turbomachinery*, GTL Report No. 205, MIT Gas Turbine Laboratory.

25. Goldman, L.J., 1972, *Supersonic Turbine Design and Performance*, ASME Paper 72-GT-63.
26. Hafez, M.M., Habashi, W.G., 1981, *Finite Element Method For Transonic Cascade Flows*, AIAA Paper 81-1472.
27. Jung, A.R, Mayer, J.F, Stetter, H, 1997, *Prediction Of 3-D Unsteady Flow In An Air Turbine And A Transonic Compressor Including Blade Gap Flow And Blade Row Interaction*, ASME Paper 97-GT-94.
28. Kopper, F.C, 1981, *Energy Efficient Engine High-Pressure Turbine*, NASA Paper CR-165567.
29. Kotiuga, P.L., Hafez, M.M., Habashi, W.G., 1983, *Computation Of Choked And Supersonic Turbomachinery Flows By A Modified Potential Method*, AIAA Paper 83-404.
30. Kotiuga, P.L., Nguyen, B.Q., Habashi, W.G., Peeters, M.F., 1990, *Finite Element Solutions Of The Navier-Stokes Equations For Compressible Internal Flows*, AIAA Paper 90-0441.

31. Kurzrock, J.W., 1989, *Experimental Investigation Of Supersonic Turbine Performance*, ASME Paper 89-GT-238.
32. Lawaczeck, O.K., 1972, *Calculation Of The Flow Properties Up And Downstream Of And Within A Supersonic Turbine Cascade*, ASME Paper 72-GT-47.
33. Liu, H.C, 1979, *Application Of 3-Dimensional Viscous Flow To Design Of Low-Aspect-Ratio* , ASME Paper 79-GT-53.
34. Manchu, G., 1987, *The Performance Estimation Of Transonic Turbine At Design And Off-Design Conditions*, ASME Paper 87-GT-148.
35. Mcgeachy, J.D., Carscallen, W.E., Moustapha, S.H, *Aerodynamic Performance Of A Transonic Low Aspect Ratio Turbine Nozzle*, ASME Journal of Turbomachinery, July 1993, pp.400-408.
36. Merz, R., Kruckels, J., Mayer, J.F, 1995, *Computation Of Three-Dimensional Viscous Transonic Turbine Stage Flow Including Tip Clearance Effects*, ASME Paper 95 Paper GT-76.

37. Monig, R, Gallus, H.E, Broichhausen, K.-D, 1987, *Off-Design Performance Of Supersonic Compresors With Fixed And Variable Geometry*, ASME Paper 87-GT-116.
38. Moustapha, S.H., *Gas Turbine Design*, Concordia university, Mech 465/616 course Handbook 1997.
39. Moustapha, S.H., Williamson, R.G., J.P. Huot, *The Effect Of a Downstream Rotor On The Measured Performance Of A Transonic Nozzle*, ASME Journal of Turbomachinery, October 1986, pp.269-274.
40. Okapuu, U., 1974, *Some Results From Tests On A High Work Axial Generator Turbine*, ASME Paper 74-GT-81.
41. Okapuu, U., Kacker, S.C, 1981, *A Mean Line Prediction Method For Axial Flow Turbine Efficiency*, ASME Paper 81-GT-58.
42. Peeters, M.F., Przybytkowski, S.M., Habashi, W.G., Hafez, M.M., 1987, *Compressible Viscous Internal Flow Calculations By A Finite Element Method*, AIAA Paper 87-0644.

43. Sari, O., Bolcs, A, 1991, *A New Base Pressure Correlation For Transonic And Supersonic Flows*, ASME Paper 91-GT-324.
44. Saxer, A.P., 1992, A numerical analysis of 3-D Stator/Rotor interactions using non-reflecting boundary conditions, GTL Report No. 209, MIT Gas Turbine Laboratory, pp.62-70, 222-230.
45. Sheridan, D.C., Amann, C.A, 1967, *Comparison Of Some Analytical And Experimental Correlations Of Axial-Flow Turbine Efficiency*, ASME Paper 67-WA-GT-6.
46. Shoemaker, M., Kwon, O., Hah, C, 1992, *A Critical Evaluation Of A Three-Dimensional Navier-Stokes CFD As A Tool To Design Supersonic Turbine Stages*, NASA Paper CP-3163-PART-2.
47. Sjolander, S.A, Yaras, M., 1989, *Development Of The Tip-Leakage Flow Downstream Of A Planar Cascade Of Turbine Blades: Vorticity Field*, ASME Paper 89-GT-55.
48. Sjolander, S.A, Yaras, M.I, 1989, *losses in The Tip-Leakage Flow Of A Planar Cascade Of Turbine Blades*, AGARD Paper CP-469 (Paper 20).

49. Sjolander, S.A, Yaras, M.I, 1990, *Prediction Of Tip-Leakage Losses In Axial Turbines*, ASME Paper 90-GT-154.
50. Sleiman, M., *Simulation of 3-D Viscous Compressible Flow in Multistage Turbomachinery by Finite Element Methods*, Concordia University, Ph.D. thesis, April 1999.
51. St'astny, M., Safarik, P., Matas, R., Jung, A.R., Mayer, J.F., Stetter, H., 1998, *Effects Of The Rotor Tip Leakage In A Transonic Turbine With Long Blades*, ASME Paper 98-GT-96.
52. Stewart, W.L., 1961, *A Study Of Axial Flow Turbine Efficiency Characteristics In Terms Of Velocity Diagram Parameters*, ASME Paper 61-WA-37.
53. Takagi, T, 1985, *Investigation Of The Aerodynamic Performance Of A Transonic Axial-Flow Turbine With Variable Nozzle*, Japan Society of Mechanical Engineers.
54. Takagi, T, 1986, *Experiments And Performance Evaluation Of A Transonic Axial Flow Turbine With Variable Nozzle*, ASME Paper 86-GT-214.

55. Tremblay, B, Kacker, S.C, Moustapha, S.H, *An Improved Incidence Losses Prediction Method For Turbine Airfoils*, ASME Journal of Turbomachinery, April 1990, pp.267-276.
56. Vlastic, E.P, Girgis, S., Moustapha, S.H, *The Design And Performance Of A High Work Research Turbine*, ASME Journal of Turbomachinery, October 1996, pp.792-799.
57. Waterman, W.F., 1976, *Measurement And Prediction Of 3d Viscous Flows In Low Aspect Ratio Turbine Nozzles*, ASME Paper 76-GT-73.
58. Wehner, M., Butikofer, J., Hustad, C.W., Bolcs, A., 1997, *Measurement And Prediction Of Tip Leakage Losses In An Axial-Flow Transonic Turbine*, ASME Paper 97-GT-203.
59. Williamson, R.G., Okapuu, U., Moustapha, S.H, 1986, *Influence Of Rotor Blade Aerodynamic Loading On Performance Of Highly Loaded Turbine Stage*, ASME Paper 86-GT-56.
60. Woinowsky-Krieger, M, Lavoie, J.P, Vlastic, E.P, Moustapha, S.H, 1998, *Off-Design Performance Of A Single Stage Transonic Turbine*, ASME Paper 98-GT-2.

Appendices

Appendix A: Turbine & gas path detailed geometry

Airfoil Mean Section Geometries

All co-ordinates are in mm.

Vane geometry		
x	suction	pressure
-17.08	14.91	14.91
-16.90	16.04	13.80
-16.72	16.49	13.36
-16.54	16.82	13.04
-16.36	17.09	12.78
-16.19	17.31	12.57
-15.29	18.06	11.61
-14.39	18.49	10.66
-13.50	18.83	9.66
-12.60	19.07	8.65
-11.71	19.19	7.62
-10.81	19.19	6.56
-9.91	19.11	5.47
-9.02	18.93	4.35
-8.12	18.64	3.19
-7.23	18.24	2.01
-6.33	17.72	0.78
-5.43	17.08	-0.48
-4.54	16.30	-1.78
-3.64	15.36	-3.12
-2.75	14.25	-4.51
-1.85	12.94	-5.94
-0.95	11.43	-7.43
-0.06	9.71	-8.96
0.84	7.78	-10.55
1.73	5.63	-12.19
2.63	3.34	-13.88
3.53	0.95	-15.62
4.42	-1.53	-17.42
5.32	-4.10	-19.28
6.21	-6.74	-21.19
7.11	-9.45	-23.16
8.00	-12.23	-25.18
8.90	-15.06	-27.26
9.80	-17.94	-29.40
10.69	-20.86	-31.60
11.59	-23.83	-33.85
12.48	-26.82	-36.17
13.38	-29.85	-38.55
14.28	-32.92	-40.99
15.17	-36.02	-43.50
16.07	-39.17	-46.08
16.96	-42.38	-48.78
17.32	-43.67	-49.61
17.50	-44.32	-49.76
17.68	-44.99	-49.84
17.86	-45.67	-49.88
18.04	-46.34	-49.87
18.22	-46.98	-49.82
18.40	-47.61	-49.73
18.58	-48.24	-49.55
18.76	-48.02	-49.02

Blade geometry		
x	suction	pressure
-7.19	0.43	0.43
-7.11	0.05	0.76
-7.03	-0.13	0.87
-6.95	-0.29	0.94
-6.87	-0.45	0.99
-6.80	-0.60	1.02
-6.40	-1.25	1.03
-6.01	-1.78	0.84
-5.62	-2.22	0.60
-5.23	-2.58	0.42
-4.83	-2.88	0.28
-4.44	-3.13	0.18
-4.05	-3.34	0.11
-3.66	-3.51	0.07
-3.26	-3.64	0.06
-2.87	-3.73	0.07
-2.48	-3.79	0.10
-2.09	-3.81	0.15
-1.69	-3.80	0.22
-1.30	-3.76	0.31
-0.91	-3.69	0.41
-0.52	-3.57	0.54
-0.13	-3.42	0.68
0.27	-3.23	0.84
0.66	-3.00	1.02
1.05	-2.72	1.23
1.44	-2.39	1.45
1.84	-2.01	1.69
2.23	-1.59	1.96
2.62	-1.13	2.25
3.01	-0.63	2.57
3.41	-0.10	2.90
3.80	0.45	3.26
4.19	1.02	3.65
4.58	1.60	4.05
4.97	2.20	4.47
5.37	2.81	4.91
5.76	3.43	5.37
6.15	4.05	5.83
6.54	4.69	6.31
6.94	5.33	6.79
7.33	5.99	7.29
7.72	6.66	7.81
7.88	6.94	8.02
7.96	7.08	8.13
8.03	7.22	8.24
8.11	7.36	8.33
8.19	7.50	8.38
8.27	7.64	8.39
8.35	7.78	8.37
8.43	7.93	8.32
8.50	8.14	8.14

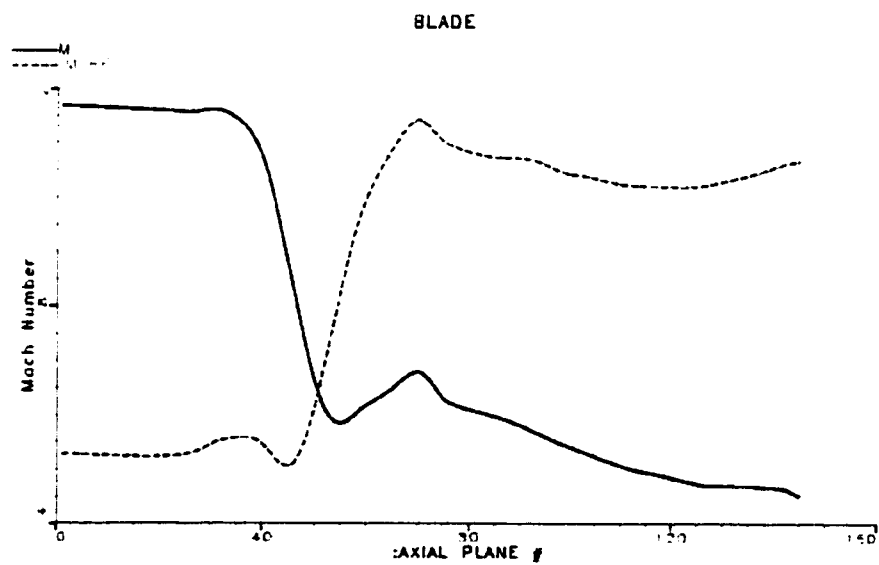
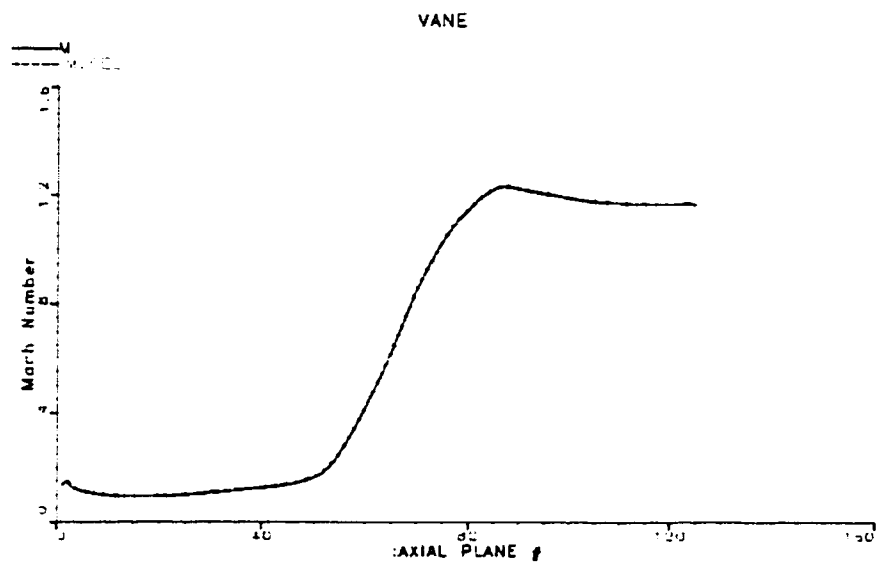
Gaspath Geometries

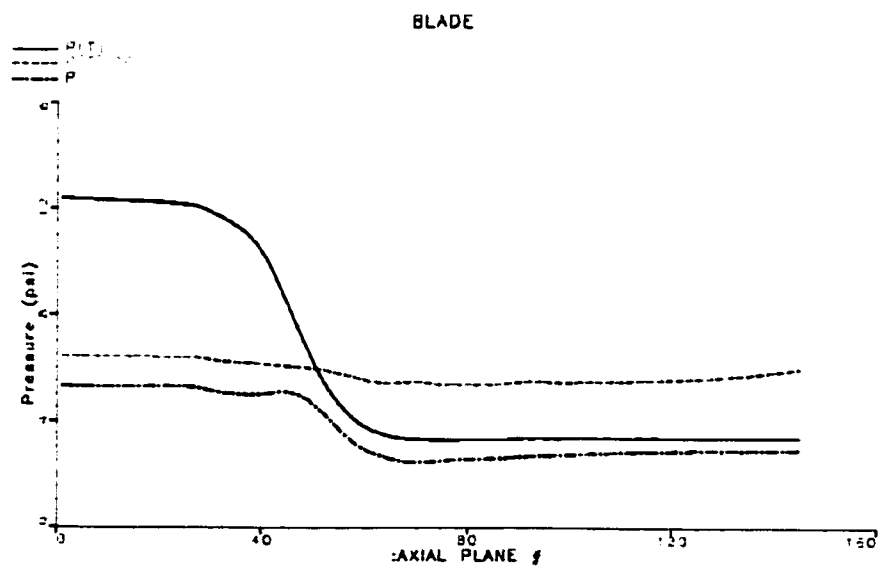
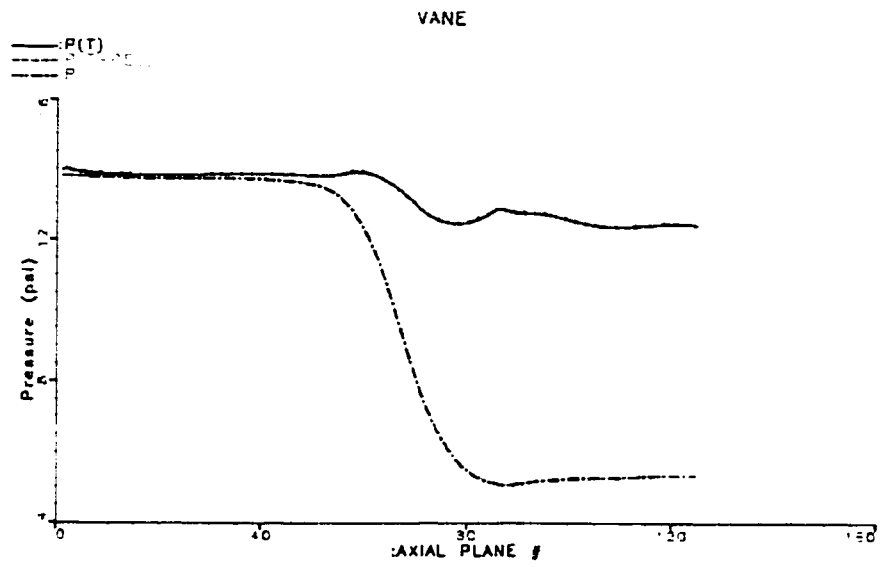
All coordinates are in mm.

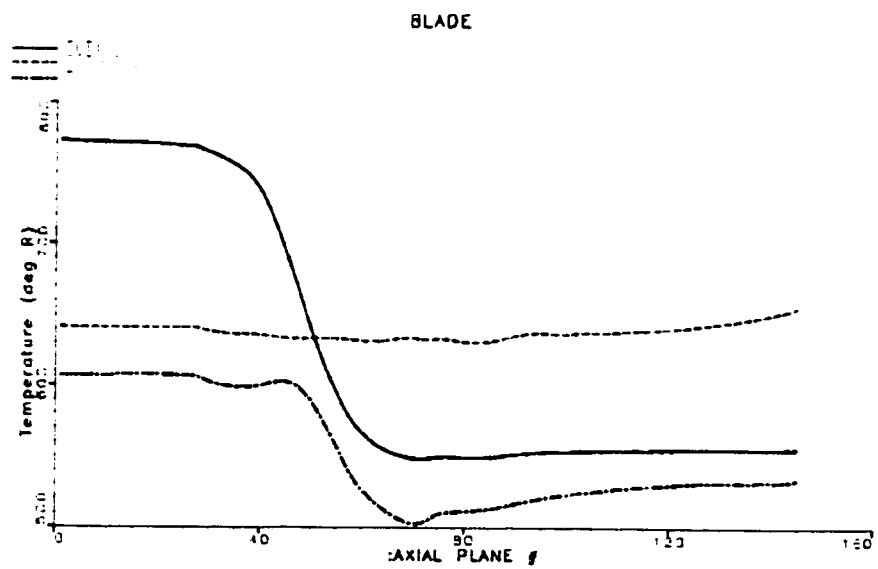
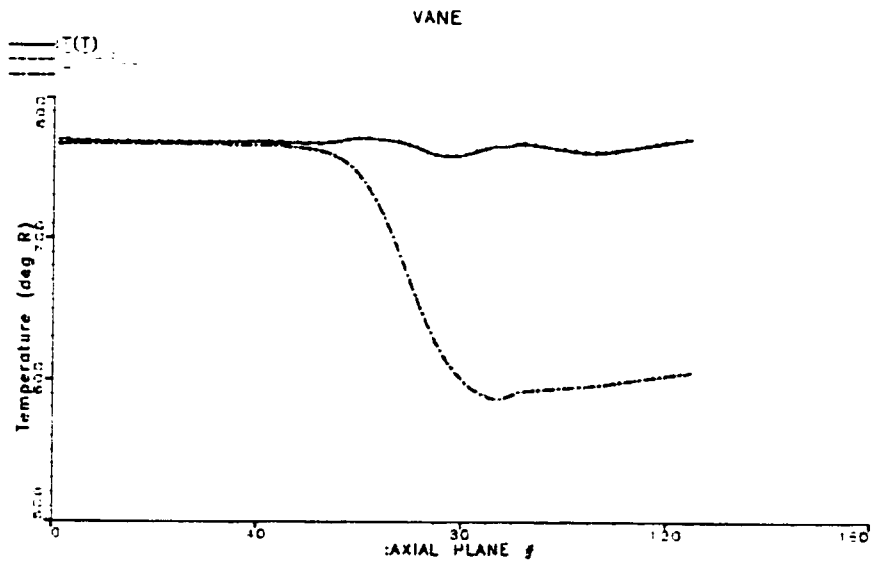
x-hub	r-hub	x-tip	r-tip
-82.81	122.66	-80.44	167.22
-80.14	122.08	-79.67	165.25
-77.45	121.59	-78.66	163.40
-74.75	121.23	-77.40	161.70
-72.02	121.03	-75.94	160.18
-69.29	120.94	-74.27	158.88
-66.56	120.94	-72.45	157.81
-63.83	120.96	-70.52	156.94
-61.09	120.94	-68.51	156.29
-58.37	120.82	-66.49	155.69
-55.64	120.58	-64.44	155.15
-52.93	120.27	-62.39	154.66
-50.22	119.91	-60.31	154.25
-47.51	119.56	-58.22	153.95
-44.80	119.24	-56.12	153.74
-42.08	118.98	-54.02	153.46
-39.35	118.79	-51.94	153.12
-36.62	118.67	-49.86	152.72
-33.89	118.62	-47.81	152.22
-31.16	118.62	-45.76	151.69
-28.42	118.66	-43.73	151.11
-25.69	118.72	-41.70	150.52
-22.96	118.77	-39.66	149.93
-20.23	118.79	-37.61	149.42
-17.50	118.76	-35.56	148.91
-14.76	118.69	-33.49	148.48
-12.03	118.69	-31.41	148.12
-9.30	118.69	-29.31	147.84
-6.57	118.56	-27.21	147.63
-3.85	118.30	-25.10	147.50
-1.19	117.71	-22.99	147.39
1.45	116.97	-20.88	147.50
4.10	116.34	-18.81	147.92
6.76	115.70	-16.74	148.35
8.65	115.20	-14.63	148.46
13.50	114.65	-12.52	148.49
15.98	114.33	-10.41	148.51
18.47	114.08	-8.29	148.54
20.97	113.90	-6.18	148.53
23.47	113.80	-4.06	148.54
25.97	113.78	-1.60	148.54
28.48	113.85	0.55	148.53
30.97	114.06	2.67	148.52
33.44	114.50	4.79	148.52
35.89	114.97	6.88	148.53
38.34	115.48	8.98	148.55
40.78	116.05	11.08	148.60
43.20	116.71	13.19	148.69

x-hub	r-hub	x-tip	r-tip
45.58	117.47	15.28	148.81
47.92	118.37	17.38	148.98
50.21	119.38	19.47	149.20
52.50	120.39	21.56	149.48
54.80	121.39	23.63	149.81
57.09	122.38	25.70	150.20
59.39	123.38	27.76	150.64
61.67	124.40	29.80	151.15
63.93	125.47	31.83	151.71
66.17	126.60	33.84	152.32
68.38	127.78	35.83	152.99
70.57	128.98	37.81	153.70
72.78	130.16	39.78	154.44
75.02	131.28	41.75	155.19
77.29	132.34	43.72	155.92
79.59	133.34	45.69	156.65
81.91	134.27	47.67	157.37
84.25	135.15	49.64	158.08
87.73	136.44	51.62	158.81
92.37	137.99	53.59	159.55
97.06	139.37	55.55	160.31
100.68	140.32	57.49	161.12
103.34	140.97	59.42	161.96
		61.33	162.85
		63.21	163.78
		65.07	164.76
		66.91	165.78
		68.72	166.86
		70.50	167.97
		72.27	169.12
		74.00	170.30
		75.72	171.51
		77.42	172.75
		79.12	174.00
		80.79	175.26
		82.47	176.53
		84.15	177.81
		85.82	179.08
		87.50	180.35
		89.13	181.57
		90.99	183.01
		92.65	184.30
		94.31	185.59
		95.93	186.85
		97.58	188.18
		99.23	189.50
		100.88	190.83
		102.53	192.14

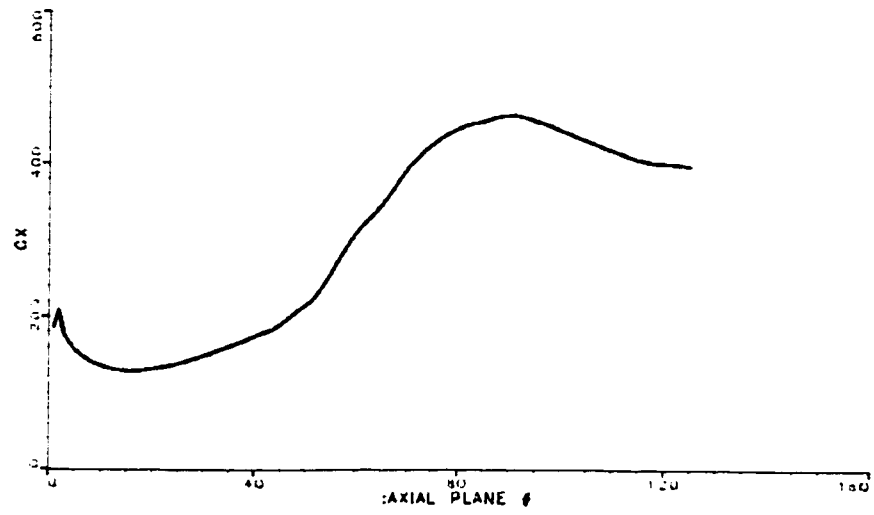
**Appendix B: Sample (the design case) thermodynamic variables
variation through out each of the vane and the blade passage**
(see Table 2.3-1 for the location of the vane and blade LE & TE)







VANE



BLADE

